

University of Windsor

Scholarship at UWindor

Electronic Theses and Dissertations

Theses, Dissertations, and Major Papers

7-7-2020

Control Strategies of DC–DC Converter in Fuel Cell Electric Vehicle

Pronay Kumar Chakrobarty
University of Windsor

Follow this and additional works at: <https://scholar.uwindsor.ca/etd>

Recommended Citation

Chakrobarty, Pronay Kumar, "Control Strategies of DC–DC Converter in Fuel Cell Electric Vehicle" (2020).
Electronic Theses and Dissertations. 8350.
<https://scholar.uwindsor.ca/etd/8350>

This online database contains the full-text of PhD dissertations and Masters' theses of University of Windsor students from 1954 forward. These documents are made available for personal study and research purposes only, in accordance with the Canadian Copyright Act and the Creative Commons license—CC BY-NC-ND (Attribution, Non-Commercial, No Derivative Works). Under this license, works must always be attributed to the copyright holder (original author), cannot be used for any commercial purposes, and may not be altered. Any other use would require the permission of the copyright holder. Students may inquire about withdrawing their dissertation and/or thesis from this database. For additional inquiries, please contact the repository administrator via email (scholarship@uwindsor.ca) or by telephone at 519-253-3000ext. 3208.

Control Strategies of DC–DC Converter in Fuel Cell Electric Vehicle

By

Pronay Kumar Chakrobarty

A Thesis

Submitted to the Faculty of Graduate Studies
through the Department of Electrical and Computer Engineering
in Partial Fulfillment of the Requirements for
the Degree of Master of Applied Science
at the University of Windsor

Windsor, Ontario, Canada

2020

©2020 Pronay Kumar Chakrobarty

Control Strategies of DC–DC Converter in Fuel Cell Electric Vehicle

by

Pronay Kumar Chakrobarty

APPROVED BY:

S. Das

Department of Civil and Environmental Engineering

M. Khalid

Department of Electrical and Computer Engineering

N. C. Kar, Advisor

Department of Electrical and Computer Engineering

April 28, 2020

DECLARATION OF ORIGINALITY

I hereby certify that I am the sole author of this thesis and that no part of this thesis has been published or submitted for publication.

I certify that, to the best of my knowledge, my thesis does not infringe upon anyone's copyright nor violate any proprietary rights and that any ideas, techniques, quotations, or any other material from the work of other people included in my thesis, published or otherwise, are fully acknowledged in accordance with the standard referencing practices. Furthermore, to the extent that I have include copyrighted material that surpasses the bounds of fair dealing within the meaning of the Canada Copyright Act, I certify that I have obtained a written permission from the copyright owner(s) to include such material(s) in my thesis and have included references such copyright to my references/bibliography.

I declare that this is a true copy of my thesis, including any final revisions, as approved by my thesis committee and the Graduate Studies office, and that this thesis has not been submitted for a higher degree to any other University or Institution.

ABSTRACT

There is a significant need to research and develop a compatible controller for the DC–DC converter used in fuel cells electric vehicles (EVs). Research has shown that fuel cells (FC) EVs have the potential of providing a far more promising performance in comparison to conventional combustion engine vehicles. This study aims to present a universal sliding mode control (SMC) technique to control the DC bus voltage under varying load conditions. Additionally, this research will utilize improved DC–DC converter topologies to boost the output voltage of the FCs.

A DC–DC converter with a properly incorporated control scheme can be utilized to regulate the DC bus voltage. A conventional linear controller, like a PID controller, is not suitable to be used as a controller to regulate the output voltage in the proposed application. This is due to the nonlinearity of the converter. Furthermore, this thesis will explore the use of a secondary power source which will be utilized during the start-up and transient condition of the FCEV. However, in this instance, a simple boost converter can be used as a reference to step-up the fuel cell output voltage.

In terms of application, an FCEV requires stepping up of the voltage through the use of a high power DC–DC converter or chopper. A control scheme must be developed to adjust the DC bus or load voltage to meet the vehicle requirements as well as to improve the overall efficiency of the FCEV. A simple SMC structure can be utilized to handle these issues and stabilize the output voltage of the DC–DC converter to maintain and establish a constant DC-link voltage during the load variations. To address the aforementioned issues, this thesis presents a sliding mode control technique to control the DC bus voltage under varying load conditions using improved DC–DC converter topologies to boost and stabilize the output voltage of the FCs.

DEDICATION

My research contributions are dedicated to my parents.

ACKNOWLEDGEMENTS

First of all, I would like to thank my supervisor Dr. Narayan Kar for his supervision and support during my post-secondary studies; by providing me continuous guidance, and plentiful resources for my study and research throughout my whole program of MASc. He always encouraged me endeavour for the best to build up a higher confidence level. Foremost, Dr. Kar treated me as a friend and family members which is a great honour to me. It was certainly a fantastic journey of research with him.

I would also like to express my gratitude and utmost respect towards my thesis committee members, Dr. M. Khalid and Dr. S. Das for agreeing to conduct on my committee and, attending my seminars and defence. Heeding their valuable comments and due suggestions, I was able to improve the quality of my overall research and this thesis.

My earnest appreciations to Dr. Shruthi Mukundan who always guided me in a supervisory role during my MASc tenure period. Second of all, Farwa who not only gave me the constructive suggestions, and feedback, but also shared her appreciated comments and explanations, which helped me to solve my research complications easily. Apart from them, one more people who always guided me from the beginning of my MASc program is Dr. Eshaan Ghosh, I am really grateful for his attitude towards research that inspires me to be meticulous to my current and future work.

TABLE OF CONTENTS

DECLARATION OF ORIGINALITY	iii
ABSTRACT.....	iv
DEDICATION	v
ACKNOWLEDGEMENTS	vi
LIST OF FIGURES	xi
LIST OF ABBREVIATIONS/SYMBOLS.....	xiv
NOMENCLATURE	xvi
CHAPTER 1 Introduction.....	1
1.1 <i>Overview</i>	1
1.2 <i>Objectives</i>	3
1.3 <i>Novelties and Contributions</i>	4
1.4 <i>Structure of the Thesis</i>	4
CHAPTER 2 Fuel Cell Equipped Electric Vehicle	6
2.1 <i>Recent Trends of Fuel Cell Electric Vehicle</i>	6
2.2 <i>Global Fuel Cell Market Review</i>	6
2.3 <i>Developments of Fuel Cell Industry in Canada</i>	7
2.4 <i>Powertrain Architecture of DC–DC Converter: Fuel Cell Electric Vehicle</i>	7
2.5 <i>DC–DC Converter Control: Interfacing Fuel Cells and Loads</i>	8
2.6 <i>System Interaction between Fuel Cell and Power Converter</i>	10
2.7 <i>Fuel Cell Equivalent Circuit for DC–DC Converter</i>	11
2.8 <i>Effects of Continuous and Discontinuous Conduction of the DC–DC Converter on Fuel Cell Performance</i>	12
CHAPTER 3 DC–DC Converter Topology for Fuel Cell Electric Vehicle	15
3.1 <i>Introduction</i>	15

3.2	<i>Overview and Main Operating Principle of Fuel Cell.....</i>	16
3.2.1	<i>Requirements for Selecting the DC–DC Converter Topology in Fuel Cell Electric Vehicle</i>	17
3.2.2	<i>Interleaved Boost DC–DC Converter</i>	18
3.2.3	<i>DC–DC Buck Boost Converter</i>	21
3.2.4	<i>KY DC–DC Converter</i>	22
3.2.5	<i>Cascade Boost DC–DC Converter</i>	23
3.3	<i>Controller for the DC–DC Fuel Cell Converter.....</i>	26
3.4	<i>Limitations of Recent DC–DC Converters.....</i>	26
3.5	<i>Conclusion</i>	27
CHAPTER 4 Controller of the Fuel Cell DC–DC Converter for Electric Vehicle		29
4.1	<i>Introduction.....</i>	29
4.2	<i>Overview of DC–DC Controller Selection Process</i>	29
4.3	<i>Dynamic Evolution Controller for Fuel Cell in EV</i>	31
4.4	<i>Boost Converter Operation.....</i>	32
4.5	<i>Dynamic Evolution Controller Design</i>	34
4.5.1.	<i>Evolution Path Selection.....</i>	35
4.5.2.	<i>Dynamic Evolution Function</i>	35
4.5.3.	<i>Analysis of Converter System.....</i>	36
4.5.4.	<i>Synthesis of Duty Cycle Formula.....</i>	36
4.5.5.	<i>PWM Duty Cycle Generation</i>	36
4.6	<i>Robust Adaptive Flatness Based Controller for Non–Ideal Boost Converter</i>	39
4.7	<i>Modeling of Non–Ideal Boost Converter</i>	41
4.8	<i>Controller Design of Non–Ideal Boost Converter</i>	43
4.9	<i>Sliding Mode Observer–Based Adaption Law Design.....</i>	43
4.10	<i>Adaptive Flatness Based Controller Design.....</i>	44
4.11	<i>Superiority of Flatness Based ControllerDesign.....</i>	46
4.12	<i>Output Voltage Regulation of DC–DC Converter: Backstepping Control</i>	47

4.13	<i>Characteristics of DC–DC Converter over Linearity & Non–linearity</i>	47
4.14	<i>FC Converter</i>	48
4.15	<i>UC Converter</i>	48
4.16	<i>Global Mathematical Model of FC: DC–DC Converter</i>	49
4.17	<i>Design of Integral Backstepping Controller</i>	50
4.18	<i>Indirect Current Control</i>	50
CHAPTER 5 Universal Sliding Mode DC–DC Converter Controller for Fuel Cell EV		53
5.1	<i>Sliding Mode Controller for Quadratic Boost Converter</i>	53
5.2	<i>Power Management System of FC: Quadratic Converter</i>	53
5.3	<i>Modeling of Quadratic Boost Converter</i>	54
5.4	<i>Controller for the Circuit Analysis (Sliding Mode Controller)</i>	55
5.5	<i>Sliding Mode Controller Based Interleaved Boost Converter for Fuel Cell System</i>	59
5.6	<i>Modeling Strategy of Interleaved Boost Converter</i>	59
5.7	<i>Interleaved Converter System Analysis</i>	60
5.8	<i>Methodology of Sliding Mode Controller</i>	61
5.9	<i>Duty Cycle Generation of PWM</i>	62
5.10	<i>Sliding Mode Control: Cascade Boost Converter for Fuel Cell Energy Generation System</i>	63
5.11	<i>DC–DC Cascade Boost Converter Model</i>	63
5.12	<i>Sliding Mode Controller Analysis</i>	65
5.13	<i>Simulation Results</i>	69
CHAPTER 6 Conclusions and Future Work		77
6.1	<i>Conclusions</i>	77
6.2	<i>Future Work</i>	78
REFERENCES/BIBLIOGRAPHY		79

VITA AUCTORIS	91
---------------------	----

LIST OF FIGURES

Figure 1.1 Annual light-duty vehicle sales per technology type, BLUE map scenario.....	2
Figure 1.2 Annual fuel cell, solar PV and wind turbine annual production: Fuel cell industry review 2017.....	2
Figure 2.1 V–I Characteristics for a single fuel cell.....	8
Figure 2.2 Inductor current for boost converter in CCM.....	9
Figure 2.3 Inductor current for boost converter in DCM.....	9
Figure 2.4 Fuel cell DC–DC converter system.....	10
Figure 2.5 V–I characteristics of a PEM fuel cell.....	11
Figure 2.6 Equivalent circuit of a PEM fuel cell.....	12
Figure 2.7 Nyquist plot for a fuel cell stack.....	13
Figure 3.1 Fuel cell DC–DC converter architecture.....	15
Figure 3.2 V–I Polarization curve of fuel cell EV.....	18
Figure 3.3 IBC with soft switching inductor converter.....	20
Figure 3.4 IBC with coupled inductor and voltage multiplier.....	20
Figure 3.5 Phase interleaved boost DC–DC converter.....	21
Figure 3.6 Phase IBC with coupled inductor.....	21
Figure 3.7 KY boost converter (inductor– coupled).....	24
Figure 3.8 KY boost converter.....	24
Figure 3.9 Integrated cascaded boost converter.....	24
Figure 3.10 Integrated soft switching cascade boost converter.....	25
Figure 3.11 Cascade boost converter.....	25
Figure 3.12 Cascade DC–DC snubber circuit.....	25

Figure 4.1 Powertrain diagram of fuel cell based electric vehicle.....	30
Figure 4.2 Conventional boost DCDC converter.....	33
Figure 4.3 Interleaved boost DC–DC converter.....	34
Figure 4.4 Exponential evolution path.....	35
Figure 4.5 PWM signal generation.....	39
Figure 4.6 Equivalent circuit of non–ideal boost converter.....	42
Figure 5.1 Power management of FC.....	52
Figure 5.2 Model of quadratic boost converter.....	54
Figure 5.3 PWM duty cycle generation	63
Figure 5.4 DC–DC cascade boost converter.....	64
Figure 5.5 The selection of fuel cell stack.....	70
Figure 5.6 Voltage controller of SMC DC–DC converter.....	70
Figure 5.7 V–I Characteristics of DC–DC converter for FCEV.....	71
Figure 5.8 The output voltage of DC–DC converter.....	71
Figure 5.9 Voltage gain.....	71
Figure 5.10 The source voltage of DC–DC converter.....	72
Figure 5.11 The stabilized load voltage.....	72
Figure 5.12 Source current of DC–DC converter enclosed by lower current ripple.....	73
Figure 5.13 Load current of DC–DC converter.....	73
Figure 5.14 Converted signal of DC–DC converter.....	73
Figure 5.15 Simulated DC–DC converter control model for PMSM.....	74
Figure 5.16 dq to phase voltage.....	74
Figure 5.17 dq to phase current.....	75
Figure 5.18 dq –axis voltage.....	75

Figure 5.19 dq -axis current.....	75
Figure 5.20 Electromagnetic torque	75
Figure 5.21 DC–DC converter control based on the rotor speed of PMSM.....	76

LIST OF ABBREVIATIONS/SYMBOLS

EV	Electric Vehicle
FC	Fuel Cell
FCEV	Fuel Cell Electric Vehicle
HEV	Hybrid Electric Vehicle
PHEV	Plug-In Hybrid Electric Vehicle
ESDs	Energy Storage Devices
PI	Proportional Integral
SMC	Sliding Mode Controller
IBC	Interleaved Boost Converter
GM	General Motors
NRC	Natural Resources of Canada
ESS	Energy Storage System
CCM	Continuous Conduction Mode
DCM	Discontinuous Conduction Mode
PEM	Proton Exchange Membrane
PEMFC	Proton Exchange Membrane Fuel Cell
SOFC	Solid Oxide Fuel Cell
AFC	Alkaline Fuel Cell
MPPT	Maximum Power Point Tracking
SR	Synchronous Rectifier

ZVS	Zero Voltage Switch
EMI	Electromagnetic Interference
PWM	Pulse Width Modulation
SiC	Silicon Carbide
IGBT	Insulated–Gate Bipolar Transistor
PFM	Pulse Frequency Modulation
PID	Proportional Integral Derivatives
DEC	Dynamic Evolution Control
MPPT	Maximum Power Point Tracking
SOC	State–of–Charge (SOC)
PMSM	Permanent Magnet Synchronous Machine

NOMENCLATURE

V_{FC}	: PEMFC output voltage (V)
I_{FC}	: PEMFC output current (A)
P_{max}	: PEMFC maximum power (W)
I_{max}	: PEMFC maximum current (A)
V_{max}	: PEMFC maximum voltage (V)
V_{DC}	: DC link voltage (V)
V_{ohm}	: Ohmic over voltage (V)
E_{Nemst}	: Open circuit thermodynamic voltage (V)
D	: Duty cycle
P	: Number of pole pairs
f_{sw}	: Switching frequency (Hz)
T_e	: Electromagnetic torque (Nm)
ξ, w_n	: Dominant damping ratio
L_d, L_q	: d - and q - axis inductance (H)
u_{sd}, u_{sq}	: d - axis and q -axis stator voltage (V)
δ	: Load angle (rad)

CHAPTER 1

Introduction

1.1 Overview

The transportation sector is essential in modern society. It is not possible in the near future to globally reduce the number of vehicles on the roads despite the environmental issues created by their considerable use [1]. To reduce critical levels of pollution, especially in larger cities, many countries have adopted strict policies towards the use of internal combustion engine vehicles. These stringent policies steer major automotive manufactures to increase investment towards the development and commercialization of hybrid (HEV), plug-in hybrid (PHEV), full electric vehicles (EVs) as well as fuel cell electric vehicles (FCEVs) [2]. Significant research has been carried out over the last decades in the area of automotive electrification to develop efficient, high-performing, safe, reliable and less costly EVs. EV research in the recent past has mainly focused on the design and optimization of electric motors, motor drives including the DC–DC converter and energy storage devices (ESDs) [3]–[5], design of powertrain component types and sizes [6], optimal control strategies [7], and battery chargers and grid charging management [8], [9], among many aspects.

Fuel cell (FC) vehicles are considered to be a promising solution that have the potential to provide clean propulsion power and increase the vehicle driving range. A few electric vehicle models powered by hydrogen FCs can be found in the market today; however, the use of fuel cells brings certain challenges that must be addressed. For example, hydrogen is flammable and explosive, and thus requires special safety issues to be addressed. Moreover, the price of FCs is still high and hydrogen fueling infrastructures must be created [10]. FCs are non-linear low-voltage current intensive power sources that must be stacked to achieve high voltage output. Due to poor-lifetime and reliability, typical output voltage is usually limited to 100 V. Nevertheless, the DC bus link of FC vehicles typically need voltage around 250–400 V [11].

Energy supplied by fuel cells has low voltage output characteristics and for any potential practical application, a step-up DC–DC converter is required. This DC–DC power converter plays an important role in FC based vehicle applications in providing the required wide voltage-gain to connect the stacks to the DC bus link. The conventional DC–DC

boost converter is typically unsuitable for such application as it presents some limitations including low efficiency. Additionally, a recent study revealed that the input current ripple of the boost converter can affect the lifetime of fuel cells [12].

According to [13], EVs available in Canada can sufficiently cover 90% of daily driving needs of the population. The predicted increase in the adoption of FCEVs will potentially cause a rise in the controller demands. The rapid progression and high penetration rates of FCEVs technologies for light-duty vehicles are necessary to achieve the strict government green house gas (GHG) emission target. [14]. Figure 1.1 shows a projection of the number of annual light-duty vehicle sales based on the technology type.

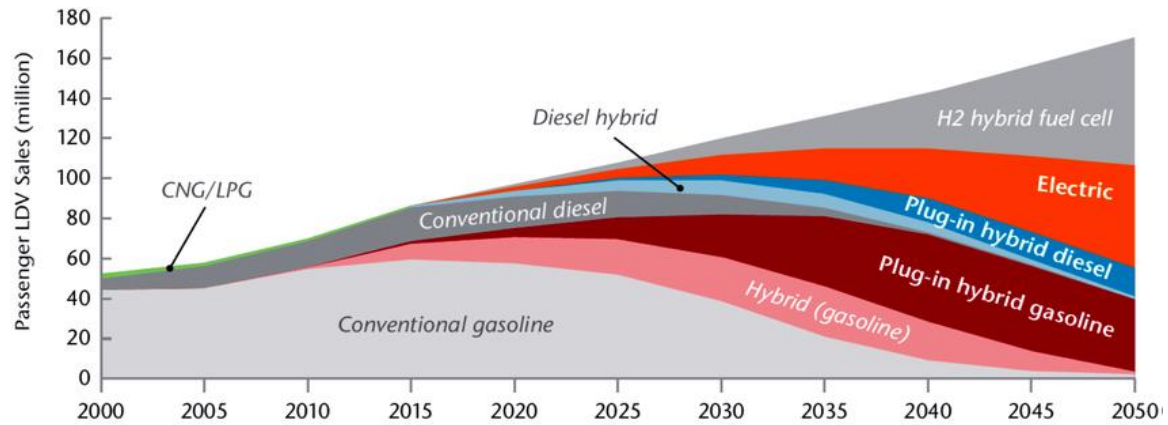


Figure 1.1. Annual light-duty vehicle sales of per technology type [14].

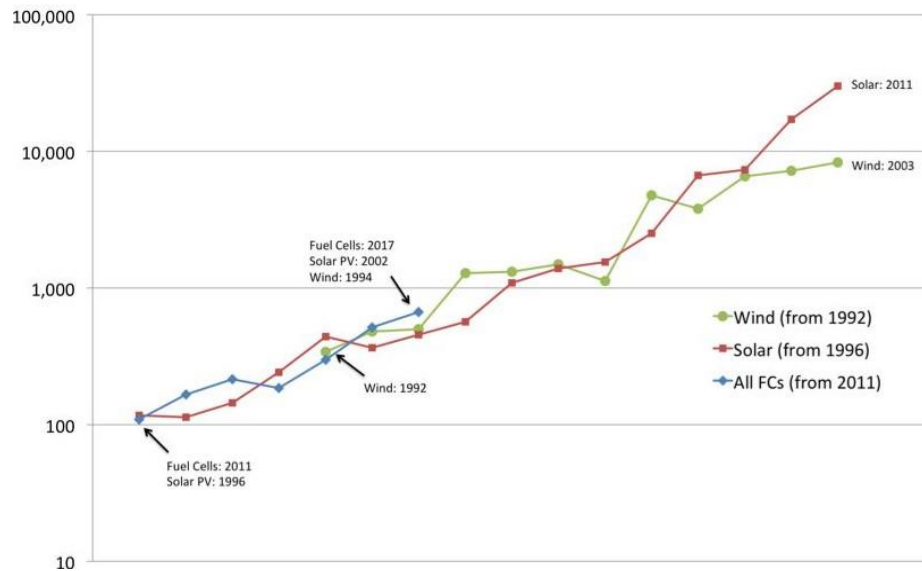


Figure.1.2. Annual fuel cell, solar PV and wind turbine annual production: Fuel cell industry review 2017 [15].

Use of FCs in power generation has also gained popularity due to rising electricity cost. Figure 1.2 displays the annual production of FCs recorded in the year 2017 in fuel cell industry review report.

1.2 Objectives

The objective of this paper is to develop a DC–DC converter control method. To accomplish this, mathematical analysis and control of the DC–DC converter for FCEVs are presented in this work. A literature survey is completed to understand the necessary improvements required to propose the control method.

Commonly used DC–DC converter control algorithms have attempted to fulfil the requirements of a FCEV. This includes the fuzzy control method. The drawback of this method is that it leads to lower control accuracy under load variations. Therefore, a robust control method is necessary to be developed to control the DC–DC converter considering the unstable output voltage characteristics.

Compared to previously mentioned algorithm for DC–DC converter control, the SMC has a simple architecture with high robustness and is widely used in EV application. This control algorithm is able to take into account internal and external parameter disturbance sensitivity. The proposed controller can ensure stability and robustness against disturbances through the utilization of a sliding mode controller. Additionally, this control method can consider uncertainties of parameters during variations of input voltage of the converter.

The selection of a suitable converter topology is crucial to overcome uncertainties of parameters during variations of input voltage of the converter. Several DC–DC boost converter topologies for the FCEV application are mentioned and discussed. This thesis proposes a universal interleaved boost converter (IBC) that interfaces the fuel cell with the vehicle powertrain. In this research, a multi–device structure with interleaved topology control is used to reduce the input current ripples, the output voltage ripples, and the size of passive components with high efficiency compared with the other topologies. In addition, low stress in the switches is expected. The proposed DC–DC converter is compared to other converter topologies to verify its dynamic performance.

Furthermore, a generalized small–signal model is derived for this DC–DC converter. The DC–DC converter topologies and corresponding controllers are designed and investigated

using MATLAB/Simulink. These simulated results have demonstrated that the proposed converter is more efficient than other DC–DC converter topologies in achieving high performance and reliability for high power DC–DC converter.

1.3 Novelties and Contributions

FC output power plays an integral role in the performance of FCEV. Power converters, especially DC–DC, is very significant in the fuel cell power system. The development of a robust control system for the converter is necessary for FCEVs.

In existing control systems for FCEVs, voltage gain is restricted and relatively unstable. The current optimization algorithm cannot improve constant power. Additionally, existing control systems have low peak power capabilities with a complex structure and unstable DC bus voltage.

The novel research presented in this thesis accounts for the aforementioned issues since it considers high gain operation for any parameter variations. The universal sliding mode controller (SMC) can be integrated with the DC–DC converter topologies depending on the rated power of the motor used in FCEV. Additionally, it can regulate the fuel cell system to deliver constant power flow. The SMC provides a stable DC bus voltage for any operating condition.

1.4 Structure of the Thesis

Chapter 2 provides a literature survey and background review of current fuel cell technology, the history, and the likely trend it will follow in the future. A review of different hybrid powertrain architectures of DC–DC converter for FCEV is provided. FC and converter techniques to solve the power flow of non-linear loads are provided. Lastly, system integration between fuel cell and DC–DC converter is discussed.

Chapter 3 outlines the DC–DC converter topology and the requirements for the selection process of a proper DC–DC converter for a FCEV. Limitations of current DC–DC converter incorporation with FCEV is explored.

Chapter 4 presents the novel controller of a DC–DC converter for FCEV. Additionally, an overview of DC–DC controller selection process for FCEV is discussed. Mathematical model of FC is established by efficient control of DC–DC converter.

Chapter 5 presents the proposed SMC of DC–DC converter as well as an analysis of DC–DC converter controllers for the FCEV.

Chapter 6 summarizes the results of this study and offers potential future work in the field on DC–DC converter control.

CHAPTER 2

Fuel Cell Equipped Electric Vehicle

2.1 Recent Trends of Fuel Cell Electric Vehicle

Fuel cell science and technology has evolved significantly in the past two decades as it is thought to be an efficient way of transforming the chemical energy of hydrogen-rich compounds into electrical energy. Although this idea of direct conversion of chemical energy to electrical energy was first demonstrated by Sir William Grove in 1839 using a fuel cell, it was only in the middle of the twentieth century when Bacon's pioneering work led to the use of fuel cell in space missions. The interest in commercialization of fuel cells for civilian use has caught up with government organizations and private corporations for the past decade because of fluctuating oil prices and environmental concerns [16]. It is well known that conventional fossil fuels, a primary source of gasoline, will not last more than a hundred years in the face of ever-increasing demand in developed and developing countries. Although reserves of natural gas, coal and tar sands may last another two to three hundred years with the current rate of production, the conversion is not efficient and pollution-free. Thus, scientists globally have taken up fuel cell development work in their quest to find a solution to the energy crises looming largely on the global population.

2.2 Global Fuel Cell Market Review

The global fuel cell market research report of 2020 is considered a comprehensive business study on this market and analyses innovative ways for business growth. Additionally, this report describes necessary factors like prime manufacturers, production worth, key regions, and rate of growth of fuel cells (FCs). This report focuses on the FC in the global market, especially in North America, Europe and Asia-Pacific, South America, Middle East and Africa. This report categorizes the market based on the manufacturer, region, type and application. Because of emission control requirements and new power line restrictions in the state's larger cities, there will be a greater motivation for fuel cell use in urban areas than in more rural areas. This concentration of fuel cells in specific urban areas will allow for more efficient utilization of fuel cell maintenance and allow for an abundance of repair technicians by utility companies. Several automobile companies including, most prominently, GM, Chrysler, and Honda, have invested hundreds of millions of dollars in

fuel cell research, development, and commercialization [17]. Each of these companies has a fuel cell prototype car currently being tested in a demonstration program.

2.3 Developments of Fuel Cell Industry in Canada

In November 2018, the Government of Canada released its Fall Economic Statement, which introduced several new energy-based initiatives which can benefit the hydrogen and fuel cell industries in the country. Canada's Department of Natural Resources (NRC) introduced the Green Infrastructure Fund in 2017 to support the efforts of industry and government entities working to deploy clean energy infrastructure solutions throughout the country [18]. Part of the fund is dedicated to electric vehicle and alternative fuel Infrastructure Deployment Initiative, a federal program seeking to construct a coast-to-coast charging network for electric vehicles, natural gas trucks, and FCVs.

2.4 Powertrain Architecture of DC–DC Converter: Fuel Cell Electric Vehicle

Recently, the usage of renewable energy resources has increased to save the environmental from various types of pollution, use of fossil fuels and to find cleaner ways to use the remaining fossil fuels. The fuel cell is gaining interest because it does not emit any pollutants and is independent of environment conditions. The fuel cells are more capable of portable applications, like vehicles, when compared to solar PV cells [19].

The typical output voltage of a fuel cell is between 0.6 V–0.7 V [20]. Therefore, a fuel cell stack typically receives a higher level of voltage. Due to this, interleaved boost converters are used for steeping-up the output of fuel cells and for reducing the ripples in input current, which are harmful to the fuel cell.

Although the FC system exhibit good power capability during steady-state operation, the dynamic response of FCs during transient and instantaneous peak power demands is relatively slow. Therefore, to improve the performance of the FC system during transient and instantaneous peak power demands in an electric vehicle application, the FC system is equipped with Energy Storage Systems (ESS). The ESS can be used to recover energy through regenerative braking [21]. For these applications, a high-power DC–DC converter is a key element that interfaces the FC or ESS with the DC bus in the powertrain of EVs. Therefore, the design of high-power DC–DC converters and their controller plays an

important role in controlling power regulation, particularly for the FC. The advantages and disadvantages of several topologies of DC–DC converters, based on their component count, are presented and compared in the existing literature as well.

2.5 DC–DC Converter Control: Interfacing Fuel Cells and Loads

Due to the low voltage that a fuel cell produces (0.7 V at nominal current), it becomes necessary to stack several of them in series to obtain a reasonable output voltage value. However, by doing so, the system becomes more complicated due to the fuel and oxygen distribution of each of the cells in the stack. Additionally, by stacking many cells in series, some thermal and water management issues arise. For this reason, the number of cells connected in series in a fuel cell stack should be maintained at a minimum. For high power applications, a stack containing between 40–50 cells is typically a good solution. Such an arrangement provides an output voltage between 400 and 800 V at full load.

Besides, the voltage produced by the fuel cell is a function of its load current exhibiting a 2 to 1 variation from no load to full load (Figure 2.1). Therefore, a step–up type DC–DC converter is required to interface the fuel cell with most electronic loads, which require a stable input voltage. DC–DC converters can operate in either continuous conduction mode (CCM) or in discontinuous conduction mode (DCM).

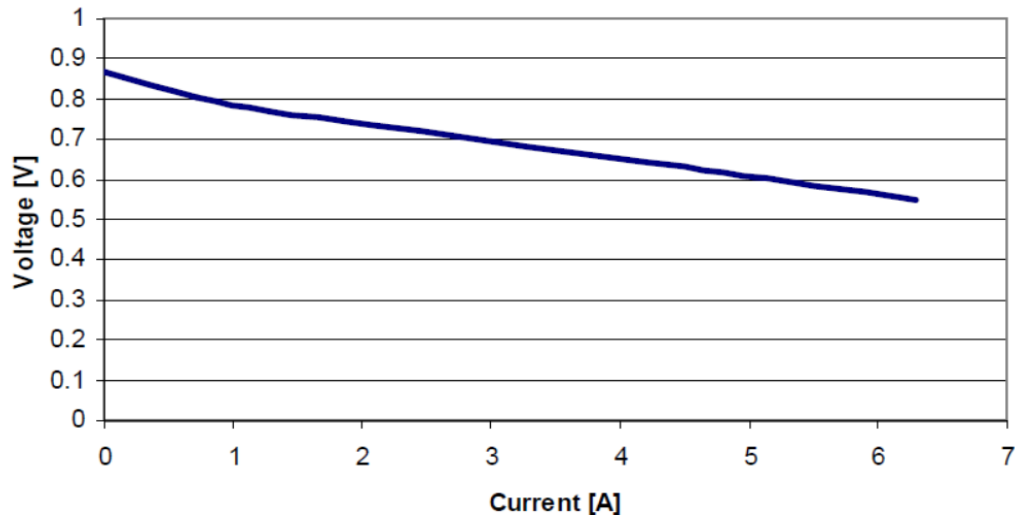


Figure 2.1. V–I Characteristics for a single fuel cell [22].

When the converter is operated in continuous conduction mode, the current being drawn from the fuel cell has small high frequency ripples as seen in Figure 2.2.

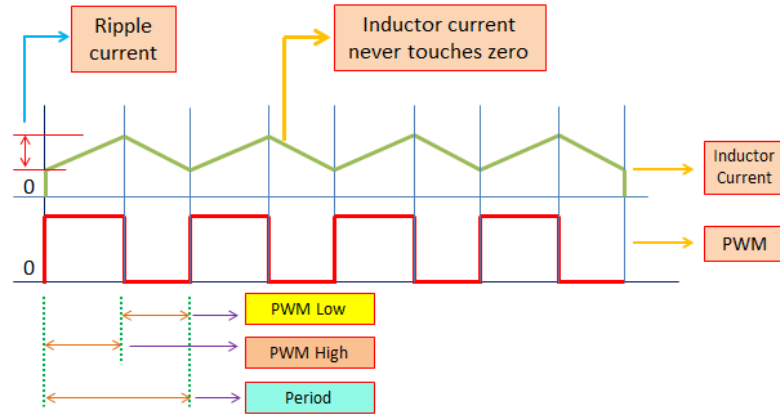


Figure 2.2. Inductor current for boost converter in CCM [23].

On the other hand, if the DC–DC converter is operated in discontinuous conduction mode, the current drawn from the fuel cell has a large high–frequency ripple (Figure 2.2).

Since fuel cells are mainly DC power sources, they are intended to supply loads that draw a DC current as seen in Figure 2.3. However, this is not the case when DC–DC converter is used. Therefore, it is necessary to analyze if the presence of high–frequency ripple currents degrades the performance of the fuel cell stack. Specifically, this analysis should include:

1. Methods to obtain an electrical equivalent circuit for a commercially available 100 kW fuel cell.
2. An evaluation of the effect of continuous and discontinuous conduction operation of the DC–DC converter on the fuel cell performance. It is important to note that discontinuous conduction operation results in smaller inductor size zero current switching during turn–on due to the absence of diode reverse recovery losses.

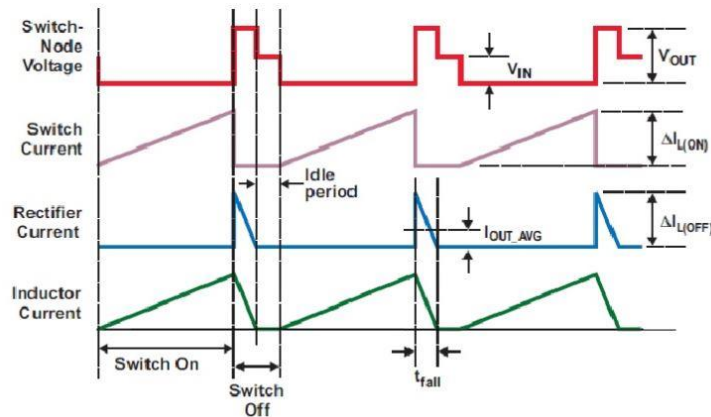


Figure 2.3. Inductor current for boost converter in DCM [23].

As mentioned before, DC–DC converters can operate in either continuous conduction mode (CCM) or discontinuous conduction modes (CCM). In the continuous conduction mode, the peak currents are lower, however, the inductor size is larger, and the effects of diode reverse recovery contribute to additional switching losses. On the other hand, the discontinuous conduction operation results in large peak currents, lower inductor size, zero current turn–on and the absence of reverse recovery phenomenon. Therefore, operating the DC–DC converter in DCM may be preferred in portable applications where size and efficiency are at a premium. However, in both cases, the current supplied by the fuel cell contains a large high frequency ripple current. The presence of these currents has an adverse effect on the performance of the fuel cell. The performance of the fuel cell can be measured in terms of the temperature rise and hydrogen fuel consumption. The result of this type of analysis facilitates the design of a DC–DC converter by providing design and optimization guidelines.

2.6 System Interaction between Fuel Cell and Power Converter

In practical applications, due to the low voltage of the fuel cell, the use of a boost type DC–DC converter is required. The interaction of the two systems must be analyzed in order to ensure proper dynamic response as well as the stability of the overall system. Normally, the control of DC–DC power supplies is carried out assuming that the impedance of the source is small enough to interfere with the operation and dynamic performance of the converter. However, the use of fuel cell as a power source, which has complex internal impedance, will alter the control characteristics of the DC–DC converter (Figure 2.4).

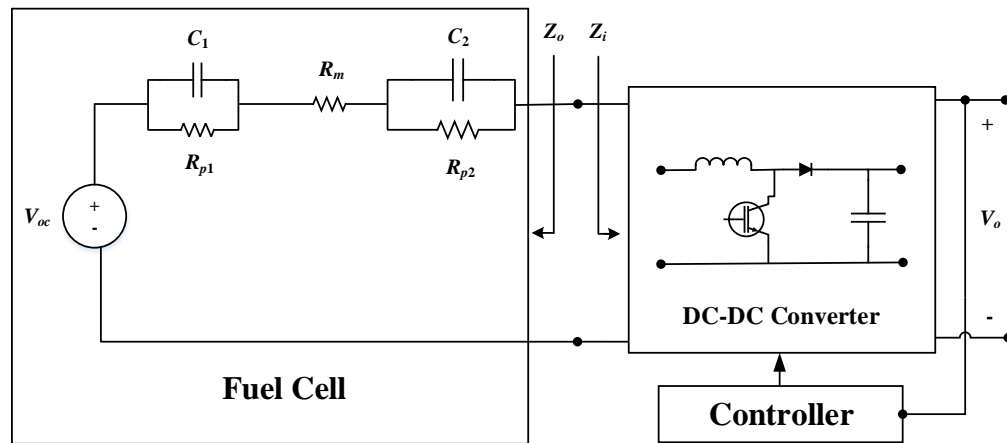


Figure 2.4. Fuel cell DC–DC converter system [24].

Thus, it is necessary to analyze the magnitude of the impact of this on the control characteristics of the system to ensure system stability and confirm that the dynamics are not degraded. By apply the tracking, it is possible to analyze the behavior of the whole fuel cell control system. For high power applications, 100 kW and higher, dead ended PEM fuel cells are normally used. In this kind of fuel cell, hydrogen enters the stack at the anode and there is a solenoid valve located at the cathode which opens at regular intervals to release the by-products of the chemical reaction. The opening of the valve is referred to as purging. During the purging interval the voltage produced by the fuel cell drops due to the reduction in internal pressure (Figure 2.5).

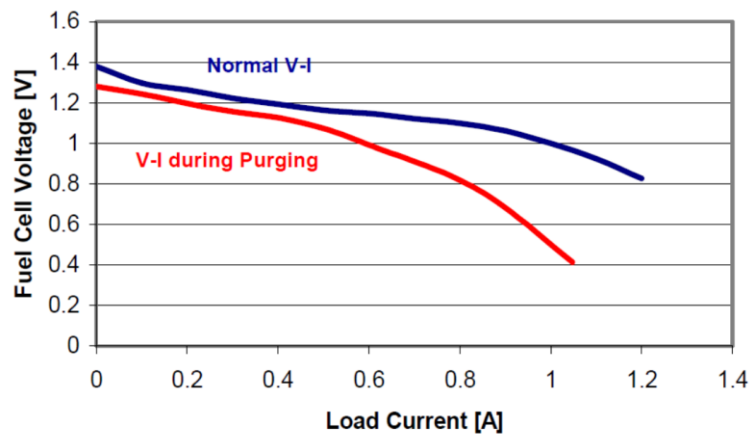


Figure 2.5. V-I Characteristics of a PEM fuel cell [25].

The magnitude of this voltage drop is a characteristic of the fuel cell and is a function of load current, fuel cell parameters, and the duration of the purging period. During the purge interval, the voltage produced by the stack is reduced. This, in turn reduces the power that the fuel cell can deliver. This may affect the stability of the fuel cell DC-DC converter system and therefore needs to be analyzed in detail.

2.7 Fuel Cell Equivalent Circuit for DC-DC Converter

Fuel cells use a chemical reaction to generate electricity, rather than storing it, as typically done with conventional batteries. Fuel cells generate electrical energy by combining oxygen with a hydrogen-based fuel, such as methanol. Power is continuous in this case while fuel and oxygen are supplied. The fuel cell can be swapped out quickly without a need to wait for recharging. Users would carry spare fuel cartridges, not extra batteries, to extend the operation and enhance convenience for this case.

Fuel cells can be considered a soft voltage source. This is due to the load-dependent nature of its output voltage. A typical fuel cell stack output voltage experiences a 2 to 1 variation from no load to full load. Additionally, since each cell in a fuel cell stack has a low output voltage (0.6 V at full load), it is necessary to stack many in series to obtain a reasonable output voltage. Stacking many cells in series adds to the complexity of the systems in terms of:

1. Complicated plumbing to uniformly distribute the fuel
2. Thermal management complexities arise when many cells are connected in series.

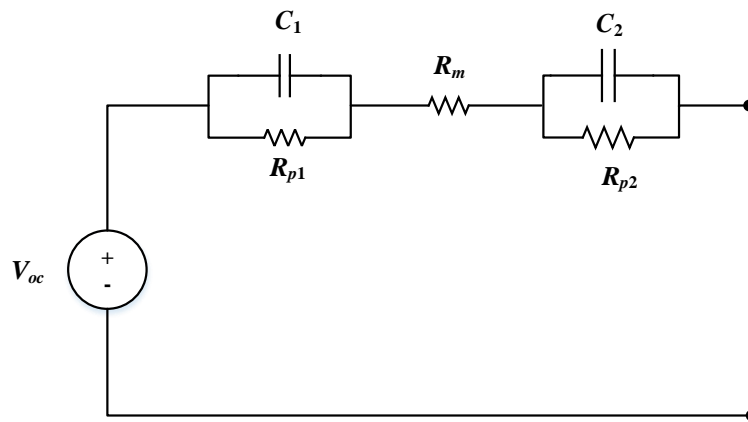
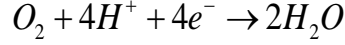


Figure 2.6. Equivalent circuit of a PEM fuel cell [25].

2.8 Effects of Continuous and Discontinuous Conduction of the DC–DC Converter on Fuel Cell Performance

Due to these limitations, a lower output voltage (3 V to 12 V) fuel cell (with fewer cells stacked in series) becomes the optimum configuration for fuel cells under 20 W. Due to the available lower output voltage, coupled with no-load to full-load variation of the fuel cell terminal voltage, a DC–DC boost converter is an ideal choice for such systems (Figure 2.6). The purpose of this chapter is to explore in depth the design considerations for the fuel cell powered electric vehicle.

The starting point is to analyze the behavior of the fuel cell stack in order to obtain an electrical equivalent circuit model. This model must provide an accurate response for steady state as well as dynamically. Over the years, many equivalent circuit models have been proposed which vary in complexity and accuracy. The chemical reactions taking place in the anode and cathode of the fuel cell are given by the following equations:



From these equations, the equivalent circuit shown in Figure 2.6 can be derived. The parameters can be obtained from the redox reactions that occur in both electrodes.

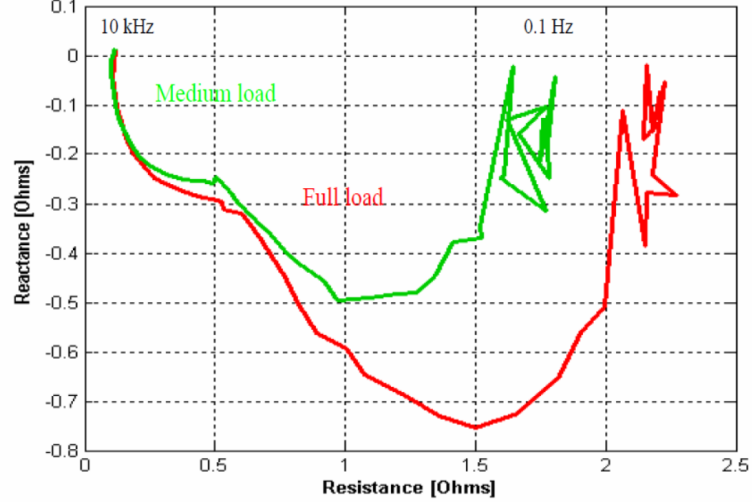


Figure 2.7. Nyquist plot for a fuel cell stack [26].

This equivalent circuit consists of the resistance of the membrane R_m , which is related to the electrolyte resistance. Also, the model contains two parallel resistor and capacitors, $R_{p1}-C_1$ and $R_{p2}-C_2$, which are the time constants of each electrode and are related to the electron transport phenomena in the anode and cathode. Specifically, resistances R_{p1} and R_{p2} model the charge transfer at the anode and cathode of the fuel cell. Comparatively, capacitances C_1 and C_2 model the capacitive effect that arises due to the electrode electrolyte at the anode and cathode, respectively. These parameters can be calculated in terms of the fuel cell chemical parameters. However, this information is rarely available for the power electronics designer.

A straightforward method of obtaining these parameters is by means of frequency spectroscopy, i.e. using a frequency response analyzer. Figure 2.7 shows a Nyquist plot obtained from a 100 kW proton exchange membrane fuel cell for different load conditions obtained through simulation by using this method. This Figure also shows the resistance and reactance of the fuel cell stack for two different load conditions and for frequencies ranging from 0.1 Hz to 10 kHz. From this plot, it is simple to identify the main elements of the equivalent circuit model. Additionally, from this result it is possible to synthesize

the parameters of the circuit model if the chemical data is not known. Each semi-circle in the graph corresponds to one R - C time constant, where the diameter of each semi-circle corresponds to its resistive value and the vertex corresponds to its characteristic frequency. The value of the membrane resistance can be obtained from the graph at the point where the reactance becomes zero.

An important point to note when designing and controlling the DC-DC converter is to know how much current ripple can be injected into the fuel cell without degrading its performance. Considering the converter, at light loads it may be more efficient to operate in discontinuous conduction mode. Additionally, designing a converter with higher input current ripple may lead to smaller inductor sizes and reduced converter size. To obtain an answer to this question, two approaches are possible to evaluate the performance; the use of the equivalent circuit model and experimental measurements. Although the analysis of the equivalent circuit is simple, it only gives information on the additional losses produced by the switching current. This can be related indirectly to temperature rise and hydrogen consumption. However, if more detailed information on these performance indexes is required, direct measurements are needed. The parameters that need to be measured include the hydrogen flow rate, which is proportional to the average power being produced by the fuel cell, and the temperature rise. Both parameters must be measured for various discontinuous conduction modes of the DC-DC converter while keeping the average output current of the stack constant.

CHAPTER 3

DC–DC Converter Topology for Fuel Cell Electric Vehicle

3.1 Introduction

This chapter reviews the evaluation of different DC–DC converter topologies for fuel cell Hybrid Electric Vehicles. The design and performance of these converter topologies are presented in terms of switching frequency, output power, component count and reliability. The crucial challenges associated with such DC–DC converter topologies are to control and obtain high efficiency for the overall performance by using a fuel cell as a principle energy source, thus integrated with the hybrid vehicle system. Therefore, it is of primary importance to select an effective converter topology suitable for fulfilling all the performance requirements. This chapter addresses different DC–DC converters topologies suits in the power conditioning system and a strategy of the controller’s selection for the fuel cell hybrid electric vehicles.

Global warming, climate change, and air quality issues alongside a dramatic increase in oil prices, has caused world–leading car manufactures like Honda, Toyota, Ford, Volvo, Chevrolet, and BMW as well as others to move towards presenting more radical fuel–efficient vehicles to the market [25]. The core concern of the automotive industry is to enhance fossil fuel efficiency and

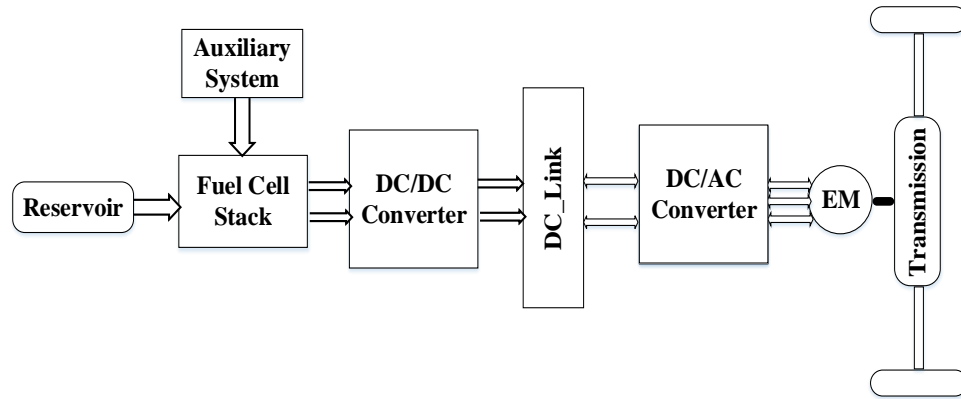


Figure 3.1. Fuel cell DC–DC converter architecture.

minimize hazardous gas emissions. Fuel cells are a promising innovation that is rapidly increasing within the hybrid electric vehicle industry [26]. Connecting the battery with the motor is required for the hybridization with the power unit and is discussed in detail within [27], [28]. The various organizations which have foreseen this on FCVs would be

financially attainable by 2020, the traditional vehicles would be supplanted by FCVs by 2030 [29], [30].

Numerous literature is accessible in the areas of the fuel cell, operation, control and application. A complete audit of fuel cell technologies, applications and challenges is referenced in [31]–[32]. Power age is one of the major fields of fuel cells. The major difficulties and chances of fuel cell use in power generation is cited in [33]. Since the fuel cell voltage is extremely low, it requires power electronic interfacing to boost up the voltage. Many power electronics converters have been developed especially for fuel cell applications. [34] provides a clear discussion regarding the power electronic interface and corresponding difficulties in the fuel cell region. The difficulties related to the control of fuel cell applications and electric vehicles are clarified in [35].

However, renewable energy supplied by fuel cells has low-voltage output characteristics and hence requires a high-performance DC–DC converter to interface the fuel cell with the load. The properties of the electrical output of fuel cells has some deficiencies like low output voltage which decreases as the load current increases, and hence requires a high step-up DC–DC converter [36], [37]. A strategy to manage power in hybrid power systems to improve the power quality while using the real power is mentioned in [38]. There are several topologies for DC–DC converters which are categorized into isolated or non-isolated topologies while adopting different switching components and switching topologies, like hard switching techniques that improve reliability and efficiency. To properly control the DC–DC converter, a good understanding of the behavior of fuel cell is important. The interaction between fuel cell and DC–DC converter must be understood in order to optimize the performance of the overall system by choosing the best control strategy. Thus, this paper provides an overview of the present status, applications and improvements in the fuel cell by using different DC–DC converter topologies. Furthermore, recent trends in the control strategies of DC–DC converters and associated issues are reported in the paper.

3.2 Overview and Main Operating Principle of Fuel Cell

The challenges and losses are explored from the V–I polarization curve [39]. The polarization curve is useful for troubleshooting issues in the fuel cell stack. If the polarization curve is recorded while increasing and decreasing the current, it may show

hysteresis losses. The voltage drops and cell operating voltage is defined in equations (3.1) and (3.2) respectively:

$$V(i) = V_{rev} - V_{irrev} \quad (3.1)$$

$$V_{cell} = V_a + V_c + V_{ohm} + E_N \quad (3.2)$$

Figure 3.2 shows the $V-I$ characteristics of a typical fuel cell where the issues of fuel cell voltage behavior are mentioned as follows: (1) The cell voltage is less than the ideal voltage, (2) There is a rapid initial fall in voltage, (3) The voltage profile is not changing linearly with current, (4) After a certain range of current densities, the voltage falls quickly [40].

Proton exchange membrane fuel cell (PEMFC) has been also described in Figure 3.2. A solid oxide fuel cell (SOFC) always requires the active and reactive power flow for robust control [41]. To overcome the slower dynamics, the sliding mode controller for a fuel cell electric vehicle has been explained in [42]. Analysis of the controller in real-time has been provided in [43]. To obtain maximum power from the fuel cell and increase efficiency, the maximum power point tracking (MPPT) algorithms can be used which is found in [44]. A convex program has been developed to optimize the power [45].

3.2.1 Requirements for Selecting the DC-DC Converter Topology in Fuel Cell Electric Vehicle

To determine the choice of a topology among the topologies presented below, the criteria described in this article must be considered. On the other hand, for a given application, the choice will be guided by the criteria of a particular application. In this case, the application is an electric vehicle using a fuel cell system. To this end, the topology must be able to operate with a low voltage-high current source with high voltage and current ripples. Also, in an electric vehicle, volume, weight and cost of the converter are very important criteria. Moreover, it is a big challenge to design a converter with high efficiency, high performance, high compactness and low cost. This limitation can be solved by using the DC converter since it can convert the source voltage from the fuel cell [46]. By reducing the operating range and the number of components, the losses of conduction dramatically reduce [47]. Another solution is to generate a nominal voltage that is equal or less than the supply voltage [48]. The converter must be capable of being balanced with the nominal supply voltage for the stepping up or stepping down [49]. Keeping this in mind, the

topology will be chosen according to some criteria that are mentioned below. For the selection of the converter topology, the following requirements are considered to obtain maximum efficiency and minimize the cost of fuel cell electric vehicles. Firstly, control of output voltage in each reference range secondly delivers current with little ripple and harmonic content. In addition, ensure the high efficiency in the whole operating range. Furthermore, incorporated by filtering and storing possibilities to improve the energy efficiency of the converter and reduce switching losses. Few isolated topologies which utilize soft-switching options can be used. On the other hand, the complexities of the converter arise due to adding this type of structure. For automotive applications, the topologies of DC–DC converters are further considered. In terms of volume, mass and fault tolerance, the DC–DC boost converter is not the best choice. In terms of reducing the fault tolerance of the converter, the addition of soft switching capabilities may not fulfill the requirement when adding to the fuel cell hybrid electric vehicle.

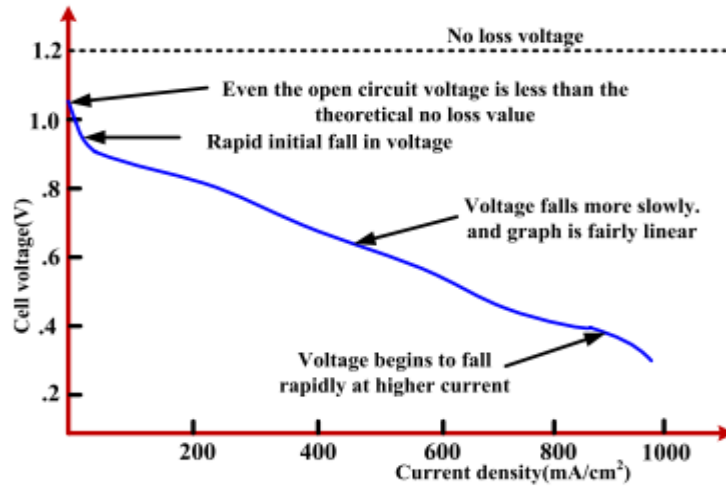


Figure 3.2. V–I Polarization curve of fuel cell EV [50].

3.2.2 Interleaved Boost DC–DC Converter

The advantages of an interleaved boost converter compared to the classical boost converter include low input current ripple, high efficiency, faster transient response, reduced electromagnetic emission and improved reliability. Four cases of interleaved boost converter have been considered and analyzed: (i) soft switching with inductor converters; (ii) IBC with coupled inductor and voltage multiplier; (iii) 4-phase IBC boost DC–DC converter; and (iv) IBC boost DC–DC converter.

The interleaved topologies easily reduce energy loss without disturbing the efficiency performance of the converters while increasing the power transformation at the same time. Figure 3.3 displays a soft switching interleaved boost converter (IBC) enclosed with single active soft-switching circuitry that is usually used for achieving the soft switching property. It contains an auxiliary switch S_a and resonant inductor L_a . C_{sa} represents the stray capacitance for the auxiliary switch [51].

$$M = \frac{V_o}{V_{in}} = \frac{1}{1 - D_{op}} \quad (3.3)$$

The operation of IBC is to enhance the power level, reduce the current ripple by using less components considering the cost of CCM mode. Figure 3.4 presents a circuit of IBC which includes a voltage multiplier cell and two coupled inductors L_{La} and L_{Lb} . The ideal voltage gain is expressed by [52]:

$$M_{ideal} = \frac{V_o}{V_{in}} = \frac{2N + 2}{1 - D} \quad (3.4)$$

Figure 3.5 shows a IBC to attain high voltage gain in DC–DC boost converter. It has the following features; the first is the minimization of current ripple and the second is an increase in the power rating with balanced efficiency which is done by regulated 90° phase delay from one to another interleaved boost converter. Voltage gain M for this circuits represent as the duty ratio of the voltage where; N is defining the winding of the motor core. Figure 3.6 presents the traditional IBC with coupled inductor. The voltage gain with four distinct operating ways is expressed as [53].

$$M_{d < 0.5} = \frac{V_o}{V_{in}} = \frac{1 + N}{(1 + N) - d(1 + 2N)} \quad (3.5)$$

$$M_{d > 0.5} = \frac{V_o}{V_{in}} = \frac{1 + N}{1 - D}$$

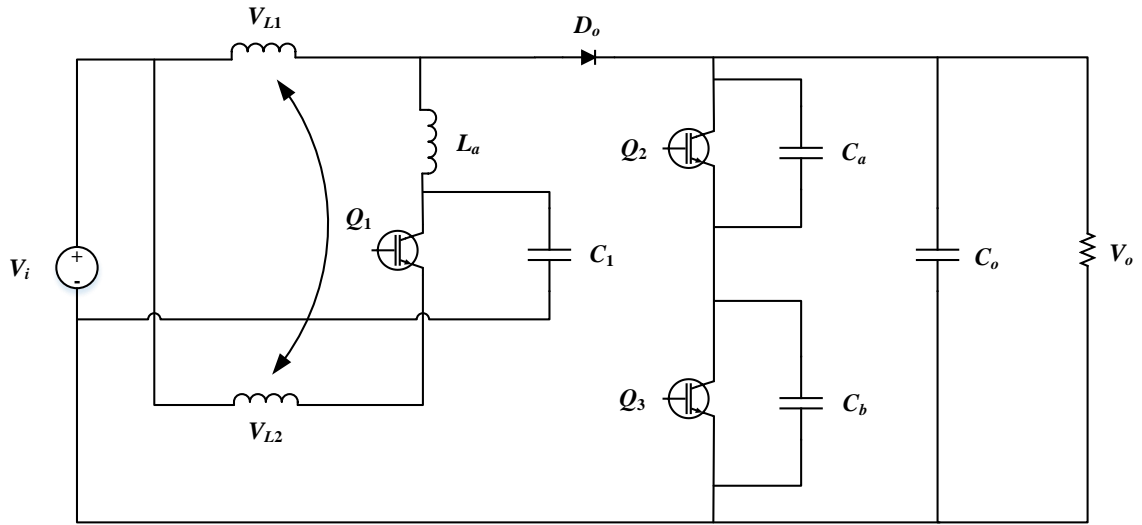


Figure 3.3. IBC with soft switching inductor converter [54].

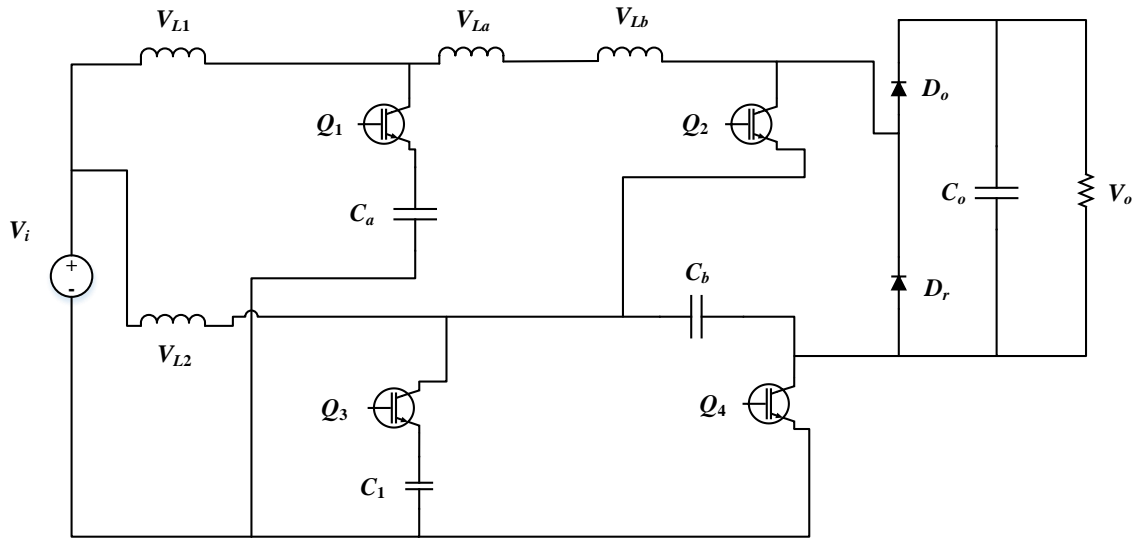


Figure 3.4. IBC with coupled inductor and voltage multiplier.

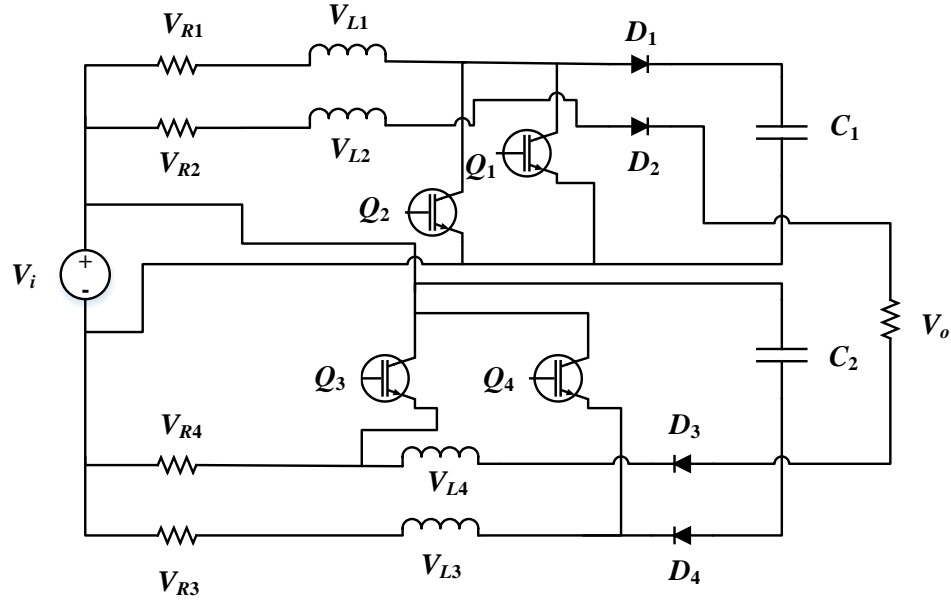


Figure 3.5. Interleaved boost DC–DC converter using 2 interconnected IBCs [54].

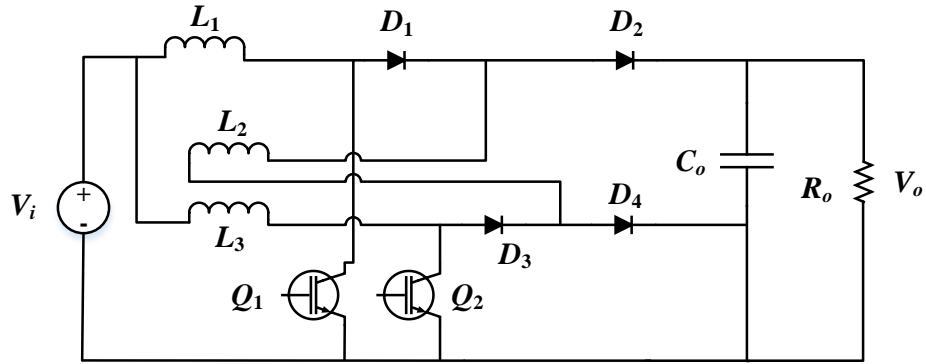


Figure 3.6. IBC with coupled inductor.

3.2.3 DC–DC Buck Boost Converter

The basic circuit of a buck–boost converter consists of a switching element, inductor, diode and capacitor. The main benefits of using this converter is its ability to produce output voltage that is equal to, less than or greater than input voltage. A switching element, along with an inductor and capacitor, makes up a simple circuit of the buck–boost converter. Depending on the position of switching element, it is easy to distinguish between either the buck or boost converter. To get a higher or lower voltage on the output, a buck–boost is most suitable. When a large current is supplied and is required to have a higher and wide

range of output levels, like in the case of an electric vehicle or any other portable application, this topology is most suitable. To familiarize oneself with the operation of buck and boost mode, for the example when the duty cycle is 0.5, the output voltage will be equal to the input voltage. The boost mode operation will be running while duty cycle is greater than 0.5. The boost mode will cause the output voltage to be higher than the input voltage. To be in boost mode, the duty cycle must be greater than 0.5 because of the lower output voltage than input voltage, for this case. Two independently controlled switches, which can work as a boost or as a buck converter, depend on the input–output condition by lowering the voltage stress of the components [55]. By using an average current controller with a simple compensation design, a low voltage, positive buck–boost converter was proposed by considering the maximum efficiency, thereby reducing the design complexity, cost and size consideration [56].

3.2.4 KY DC–DC Converter

KY boost converter possesses fast transient responses, which are like the buck converter with synchronous rectification. It possesses non pulsating output current, which not only decreases the current stress on the output capacitor, but also reduces the output voltage ripple. Similar to other conventional converters, the KY converter is used to boost the voltage based on its quick transient response [57]. The voltage gain M can be expressed as:

$$M = \frac{V_o}{V_{in}} = 1 + D \quad (3.6)$$

The main advantage of this converter is the minimization of current stress on the load demand. Figure 3.7 presents a boost converter of KY which is a combination of a traditional SR boost converter and the basic KY converter. In the KY converter, the input is replaced by one buffer capacitor C_m , whereas in case of SR boost converter, the buffer capacitor C_m is put in a place of output. The voltage gain M for the KY boost converters is denoted as [58].

$$M = \frac{V_o}{V_{in}} = \frac{2 - D}{1 - D} \quad (3.7)$$

The KY boost converter has a greater voltage transformation ratio than the conventional SR boost converter by using its continuous conduction mode (CCM). It has a higher level of efficiency, approximately 90%, when used in a low–ripple current application. Figure

3.8 represents a KY boost converter with a coupling inductor expressed in [59]. Comparing to previous KY converters, it has an efficiency which is higher than 90%.

$$M = \frac{V_o}{V_{in}} = \frac{2}{1-D} + \frac{N_s}{N_p} \quad (3.8)$$

3.2.5 Cascade Boost DC–DC Converter

In hard switching, the cascade connection of two boost converters can show a higher efficiency than the conventional quadratic boost converter since the diode, which replaces the IGBT in the input stage of the quadratic boost, must support high voltage and high current. However, by using SiC in IGBT and diodes, the simplicity of the quadratic boost converter becomes more apparent. The dynamical behavior at same operational conditions remains approximately the same. Alternatively, the cascade boost converters have two controlled switches. From this, it is possible to use two different duty cycles to accomplish some control objectives or find a maximization of the efficiency. Due to a lack of high step-up necessities, the voltage gains and the large current ripple of the traditional boost converter, cascade DC–DC converter is used to fulfil the disadvantages of the conventional boost converter. However, from a control circuit viewpoint, the cascaded boost converter is very complicated when compared to a quadratic boost converter. Moreover, regarding different switching frequency of switches, the design process of the Cascaded Boost converter is very difficult. Figure 3.9 shows the typical structure of a cascade boost converter. To minimize system complications, the cascade boost converter has the capability of integrating two or more switches in a single switch [60]. However, Figure 3.10 presents an integration of cascade DC–DC boost converter with the soft switching of ZVS [61]. In Figure 3.11, a converter which includes the CCM mode with minimum conduction losses has been presented. This converter has three intervals; during its very first cycle, L_1 and L_2 get charged when M_1 and M_2 are on. On the second cycle, L_2 get discharged while M_2 is turned off. In the third cycle, M_2 is turned on and M_1 turns off [62].

$$M = \frac{V_o}{V_{in}} = \frac{1}{(1-D_1)(1-D_2)} \quad (3.9)$$

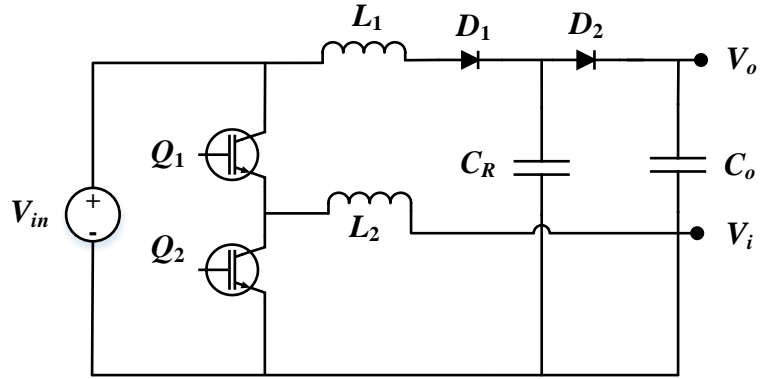


Figure 3.7. KY boost converter (Inductor-Coupled) [63].

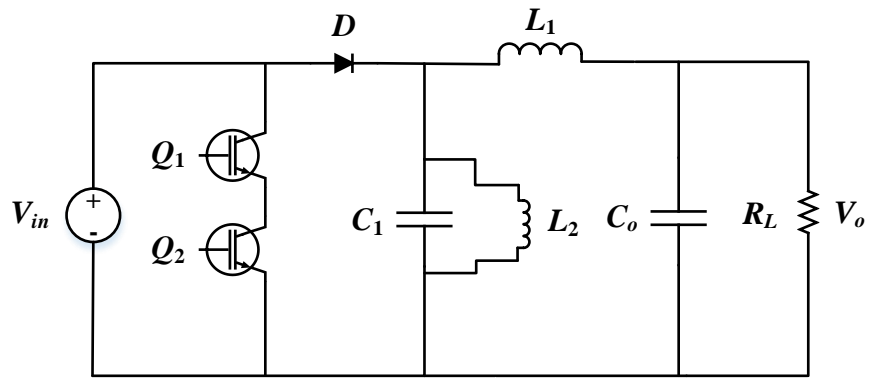


Figure 3.8. KY boost converter.

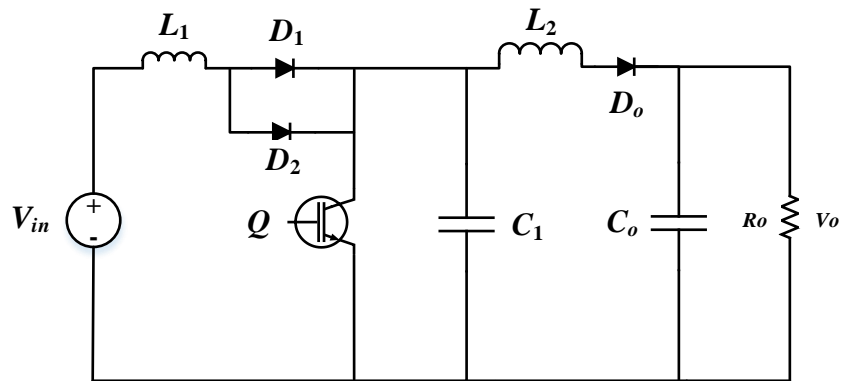


Figure 3.9. Integrated cascaded boost converter [63].

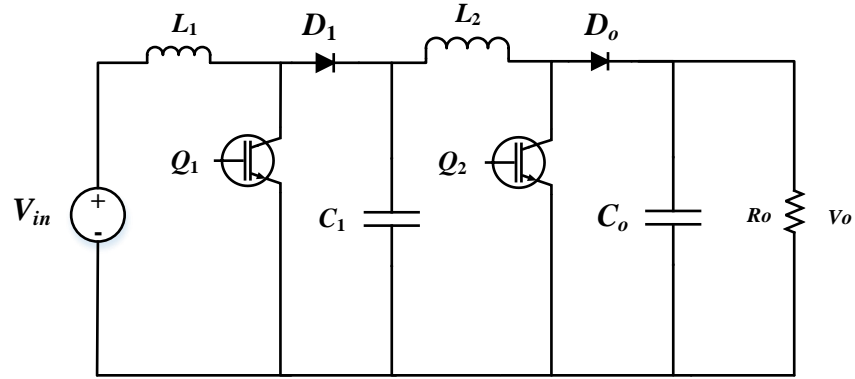


Figure 3.10. Integrated soft switching cascade boost converter.

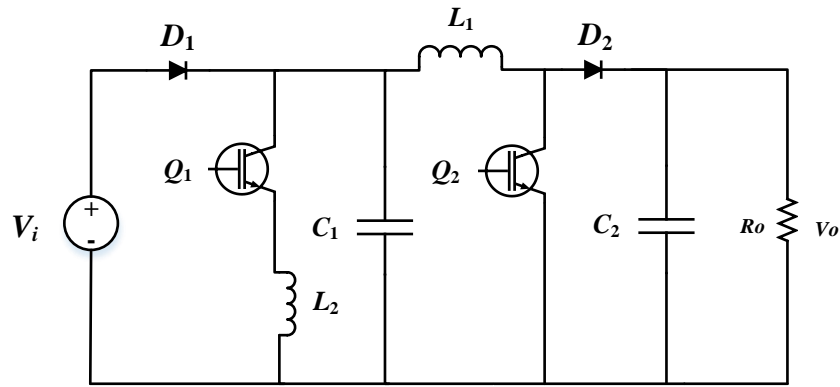


Figure 3.11. Cascade boost converter.

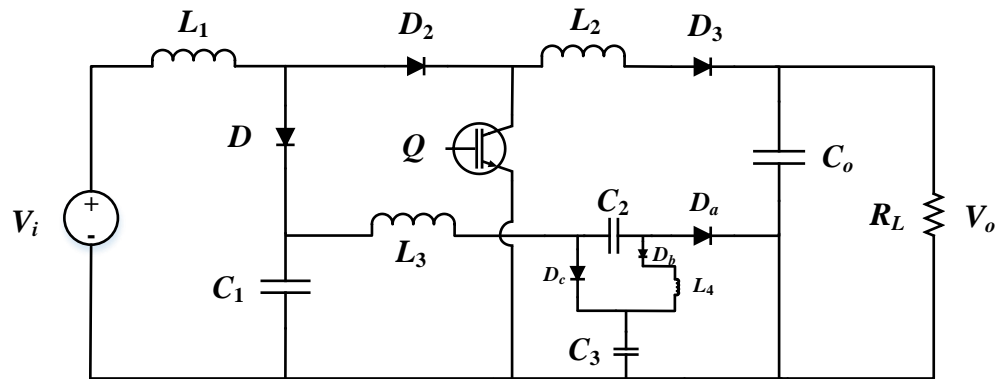


Figure 3.12. Cascade DC-DC snubber circuit [64].

The main advantage of this is having very low conduction losses of semiconductor devices and high input current along with low voltage stress.

Snubber circuit is usually helpful to dim the large voltage spikes of the main switches since it uses the resistor capacitor diode (RCD) which is presented on Figure 3.12. It has

additional power loss due to leakage inductance. This can be solved by using a passive snubber which is cited in [64]. The voltage gain M of this type of converter is expressed as:

$$M = \frac{V_o}{V_{in}} = \frac{1 + n_1 D}{1 - D} \quad (3.10)$$

3.3 Controller for the DC–DC Fuel Cell Converter

Power electronic converters in general and DC–DC converters have great importance on control performance and the efficiency of the energy production process based on fuel cells. The control of the operation point of fuel cells requires the appropriate use of DC–DC converters, capable of providing accurate support to the control methods. The main objective to be achieved when applying the converters to fuel cells is obtaining maximum efficiency while using the most appropriate control strategies, considering the requirements of the output. For instance, the control scheme of the traditional PWM converter should be designed to satisfy the current and voltage requirements. A simple feedback PI controller is usually used to maintain a constant bus voltage by the requirement in converter output, irrespective of the variations in load and input voltages. As was concluded by the authors in [65], [66], the dual-loop control strategy is more efficient than other techniques to achieve high performance for the PWM converters as illustrated through the block diagram of the control strategy. Similarly, the use of a cascaded structure can lead to intersections between the control of the two converters where the impedance criteria are often used to study the stability of the cascaded system [67], [68] and the two converters are considered by the controllers.

In recent times, controllers that use neural networks and fuzzy logic-based controller for the DC–DC fuel cell application are becoming popular because of its convenient multi-control options. The automatic turning capability and flexibility that is currently present allows the neural optimal controller for the fuel cell to be integrated into the fuel cell for its intelligent model in most hybrid electric vehicle applications [69]. The output voltage of this converter can be regulated to zero voltage switching DC–DC and the DC link voltage can be stabilized by using special techniques of fuzzy logic [70], [71].

3.4 Limitations of Recent DC–DC Converters

When the output power is too high and the input current is also excessive, the traditional boost converter has a voltage collapse point which is usually turned on by reducing the

input current. This, in turn reduces the efficiency of the converter. For low voltage applications, replacing the diode with a switching element can improve the efficiency. However, this results in large voltage drops across the diode. A shoot-through current between the turn on and turn off can be used in case of time delay of the circuit.

Pulse width modulation (PWM) and pulse frequency modulation (PFM) control are used to achieve a high frequency, but the converter might have different power losses such as conduction and switching losses. The main obstacle of a boost converter includes the high switching noise which generally presents when turning on and off the switching element. This declines the quality of the output voltage and degrades the performance of the fuel cell [72]. Additionally, due to hard switching, the PWM suffers from high device stress, high switching losses and objectionable EMI when used at a high switching frequency that is similar with the soft-switching PWM techniques that is typically used for greater switching frequency operation with high efficiencies and larger ratios.

3.5 Conclusion

This chapter presents a detailed review of fuel cell dependent DC–DC converter. In addition, the operating principle of fuel cell DC–DC converter was explored as well as the current research challenge in fuel-based DC–DC control topologies that can be used for fuel cell applications like electric vehicles (EV), power generation, spaceships etc. As mentioned, the research challenge in this chapter is to incorporate any topologies of DC–DC converter for the better control and utilization of the fuel cell technology efficiently. A literature survey on DC–DC converters point out that they can be used to produce more efficient conversion of power from the fuel cell to the load by using a DC converter or a combination of DC converters. By doing so, this can easily address major limitations like low voltage, unregulated voltage, unstable power and low current density. Various topologies which are issued in previous papers are discussed and compiled in this paper. Above all, the limitations and drawbacks of the traditional boost converter is also discussed for the fuel cell hybrid electric vehicle.

The topology using for the control of DC–DC on fuel cell electric vehicles can be divided into two stages; in the single stage, the DC converter is stand alone, but the AC converter is needed in the multistage topologies. Additional studies on the perfection of new topologies can be done for the DC–DC converters control even including new switching

techniques which are also required to create a higher efficiency and progress the existing switching strategy.

CHAPTER 4

Controller of the Fuel Cell DC–DC Converter for Electric Vehicle

4.1 Introduction

The fuel cell has great potential to become the main candidate for providing electrical energy in the coming years. High efficiency, high current density, trivial pollution and low noise are the important advantages of fuel cells which will allow it to become a popular energy source in the future. The fuel cell is essentially a generator that uses hydrogen fuel to produce a quick response. It allows a fast start–up under low operating temperatures. Fuel cells produce no pollution and this meets the needs of environmental protection systems. However, there are a few shortcomings of fuel cells. For instance, the fuel cell has no storage capacity of energy, slow dynamic response, unstable output voltage, cold start problem and so on. For fuel cells with low voltage and low power, the output voltage varies greater at different times. Namely, its feature is very soft. To realize a steady DC power supply using the fuel cell, DC–DC converter is usually needed to improve the soft characteristics of the output voltage of the fuel cell.

4.2 Overview of DC–DC Controller Selection Process

For the reason of low contamination and having an abundance on the earth's surface, hydrogen is the most common fuel used for many fuel cells. Different types of fuel cells such as alkaline fuel cell (AFC), solid oxide fuel cell (SOFC) and proton exchange membrane fuel cell (PEMFC) are typically used currently as described in [73]. The compensations and shortcomings of these types are described in the literature sections. Among several fuel cell technologies, the PEM fuel cell is very useful in a wide range of applications [74]. The PEM fuel cell is one of the most promising technologies as an alternative power source of an electrical power generation system since it can offer a host of benefits including low cost and long cycle life. [75].

However, a standalone FC system integrated with an automotive power train is not always enough to provide the load demands of a vehicle. This is true during the initial peak power during transients such as start–up, acceleration or sudden change in load. Additionally, it cannot take advantage of the regenerative power of an electric vehicle at braking. However, a sliding mode controller (SMC) is elaborated to regulate the output voltage based on the demanding power and to ensure the stability of the overall system [76]. This does not match

with reality since all FCs are autonomous and dependent on their specific energy storage [77]. This is why DC–DC converters with an SMC control strategy are used [77]. The control and the power management using DC–DC converters ensure and maintain the DC output voltage at a constant value to feed the fuel cell. This is since the DC–DC converters have the objective of converting power in an appropriate form.

There are several hundreds of topologies for DC–DC converters interfacing with the fuel cell electric vehicle applications, and few numbers of a control scheme for the control of the power output. Most of the controllers can provide a DC output voltage controlled with pulse width modulation (PWM) switching techniques. This is typically the main reason for greater switching losses and the increase of ripple current in both the input and load side. These lead to a decrease in the overall efficiency.

To increase the efficiency and rated output power, a sliding mode controller is used for power management due to some other advantages as presented in [78]. Among others, the implementation simplicity and great performance in different fields, such as electric vehicle motor control and robotics by time-varying capability of the system for robust stabilization make the sliding mode controller advantageous [79].

The proposed algorithm of SMC is capable of stabilizing the fuel cell storage system over the entire operating range by maintaining the robustness of the system and providing better tracking accuracy than traditional controllers in a relatively simpler way with just changing the gain of the sliding surface.

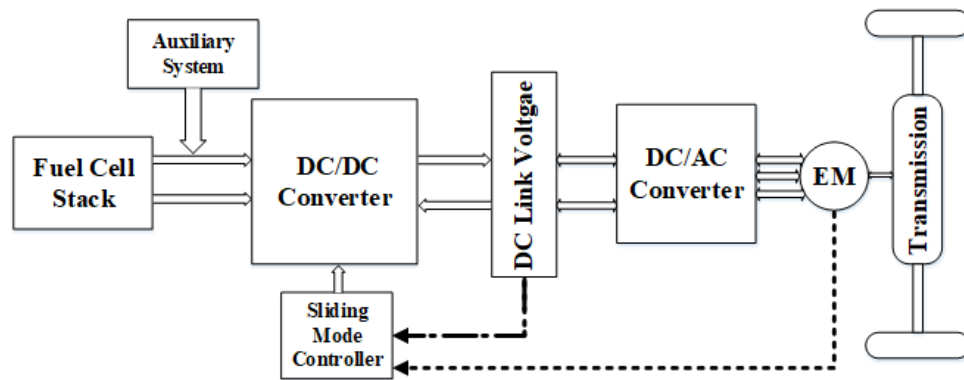


Figure 4.1. Powertrain diagram of fuel cell based electric vehicle.

4.3 Dynamic Evolution Controller for Fuel Cell in EV

High power and high voltage boost DC–DC converters are needed for providing the interface between the fuel cell energy and high voltage DC–link bus of the inverter [80]. In these applications, the high power boost converters are required to step up the voltage of FCEV output voltage to the DC–link bus voltage.

In such applications, it becomes challenging to maintain high efficiency using a conventional boost converter. At the same time, for high power applications like an electric vehicle, the low input voltage causes large input current to flow. Additionally, with low duty cycle operation, the ripple current running through the diodes and the output capacitor becomes very high. All of these increase the losses enormously and make the conventional boost converter inefficient. The use of switches with higher blocking voltage rating, leads to more losses because of the parasitic elements present in the circuits that induce additional voltage stresses and necessitate.

The major challenge of designing a boost converter for high power applications is how to handle high current at the input and high voltage at the output. An effective way is to parallel the inputs of the boost converter for input current sharing [81]. Based on this concept, an interleaved boost DC–DC converter is a suitable candidate for stepping–up the voltage on high power applications [82].

Given the controller, the need for an efficient controller for interleaved boost DC–DC converter has increased. Since boost converter is a non–linear time–varying systems [83], the design of controllers must have the capability to cover up the nonlinearity and time–varying properties of the system.

In this chapter, a new approach for interleaved boost converter controller’s synthesis, based on dynamic evolution control theory is presented. The proposed dynamic evolution control exploits the non–linearity and time–varying properties of the system to make it a superior controller. This control tries to overcome the aforementioned problem of linear control by explicitly using the dynamic equation model of the converter for control synthesis. Synthesis of dynamic evolution control when applied to boost DC–DC converter is discussed.

4.4 Boost Converter Operation

A. Conventional Boost DC–DC Converter

The schematic diagram of the conventional boost DC–DC converter is shown in Figure 4.2. The duty cycle D , is defined as the time relationship that the switch is on relative to the total switching period. Based on steady state analysis, the DC voltage in the inductor V_L can be expressed as (4.1) and is equal to zero [84].

$$V_L = D(V_{in}) - (1 - D)(V_{in} - V_o) = 0 \quad (4.1)$$

From (4.1), at steady state it can be verified that the gain ratio between output and input voltage becomes:

$$M = \frac{V_o}{V_{in}} = \frac{D}{1 - D} \quad (4.2)$$

The inductor current can be obtained by the input and output power:

$$I_L = \frac{V_o}{V_{in}} \cdot I_o \quad (4.3)$$

Substituting (4.2) into (4.3), the inductor current can be expressed as:

$$I_L = M \cdot I_o \quad (4.4)$$

From (3), the inductor current of boost converter will increase proportionally to the output power, while (4.4) says the boost converter inductor current also will increase with the increase of the voltage gain ratio M . These result in a high inductor current of the boost converter at high power applications. This makes the conventional boost converter inefficient for high power applications.

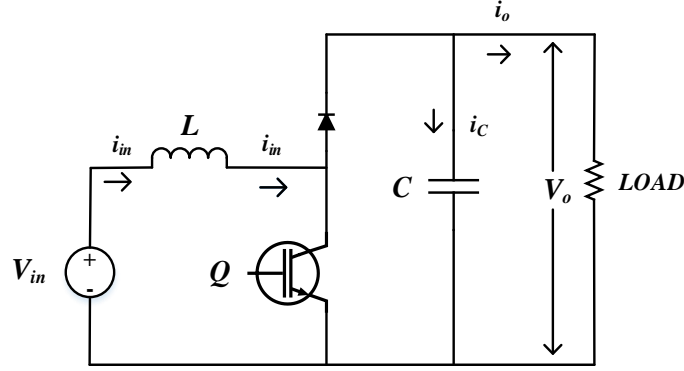


Figure 4.2. Conventional boost DC–DC converter [84].

B. Interleaved Boost DC–DC Converter

The interleaved boost DC–DC converter is proposed to deal with the high current problems at high power applications. Figure 4.3 shows the schematic diagram of the interleaved boost DC–DC converter, consisting of two parallel–connected units, which are controlled by a phase–shifted switching function (interleaved operation).

The interleaved boost DC–DC converter can operate in two modes, continuous current mode (CCM) and discontinuous current mode (DCM). In this paper, the converter is assumed to operate in CCM mode.

In order to simplify the calculation, it is assumed that the inductance value of both inductors is L_1 and L_2 , where $L_1 = L_2 = L$, and the duty cycle of Q_1 and Q_2 is denoted as D_1 and D_2 , with $D_1 = D_2 = D$. According to Figure 4.3, the operation of the CCM modes are explained as:

(1) State a:

At time t_0 , Q_1 is closed and Q_2 is opened. The current of the inductor L_1 starts to rise, while L_2 continues to discharge. The rate of change of i_{L1} is $di_{L1}/dt = V_i/L$, the rate of change of i_{L2} is $di_{L2}/dt = (V_i - V_o)/L$.

(2) State b:

At time t_1 , Q_1 and Q_2 are opened. The inductors L_1 and L_2 discharge through the load. The rate of change of i_{L1} and i_{L2} are $di_{L1}/dt = di_{L2}/dt = (V_i - V_o)/L$.

(3) State c:

At time t_2 , Q_2 is closed while Q_1 still opened. The current of the inductor L_2 starts to rise, while L_1 continues to discharge. The rate of change of i_{L2} is $di_{L2}/dt = V_i/L$, while the rate of change of i_{L1} is $di_{L1}/dt = (V_i - V_o)/L$.

(4) State d:

At time t_3 , Q_2 is opened and Q_1 still opened. The situation is same as state b. The inductors L_1 and L_2 discharge through the load. The rate of change of i_{L1} and i_{L2} are $di_{L1}/dt = di_{L2}/dt = (V_i - V_o)/L$. Due to the symmetry of the circuit, the next state is similar to the previous.

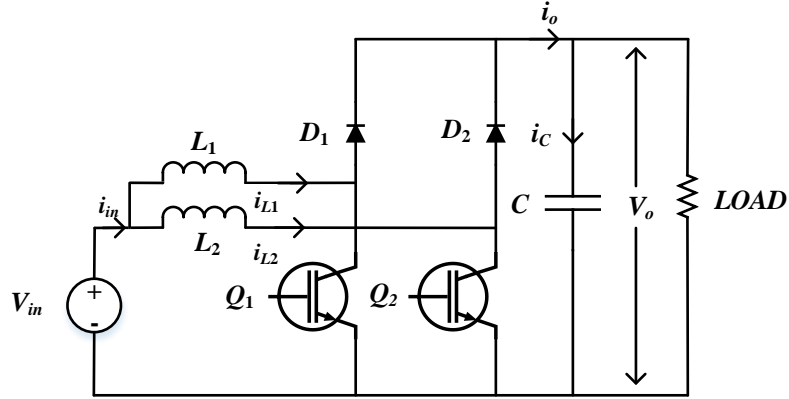


Figure 4.3. Interleaved boost DC-DC converter.

4.5 Dynamic Evolution Controller Design

Dynamic evolution control is a new control technique in power electronics applications. The basic idea of dynamic evolution control is to reduce the error state by forcing the error state to follow the specific path which ensures that the error state goes to zero with an increase of time. This specific path is named the Dynamic Evolution Path. By using dynamic evolution control, the dynamic characteristic of the system is forced to make evolution by following an evolution path.

Design steps of the DEC based controller can be described in five steps as follows:

1. Evolution path selection

2. Dynamic evolution function
3. Analysis of the converter system
4. Synthesis of duty cycle formula
5. PWM duty cycle generation

4.5.1. Evolution Path Selection

The first step in the DEC based control design is to determine the evolutionary path that ensures that the error state will go to zero at any increase of time. In this research [85], the evolution path is an exponential function as shown in Figure 4.4. With this evolution path, the value of the dynamic characteristic of the system will decrease exponentially to zero by an equation.

$$Y = Y_o \cdot e^{-mt} \quad (4.5)$$

Where, Y is the dynamic characteristic of the system, Y_o is the initial value of Y , and m is a design parameter specifying the rate of evolution.

4.5.2. Dynamic Evolution Function

The dynamic evolution function of this controller can be written as:

$$\frac{dY}{dt} + mY = 0, m > 0 \quad (4.6)$$

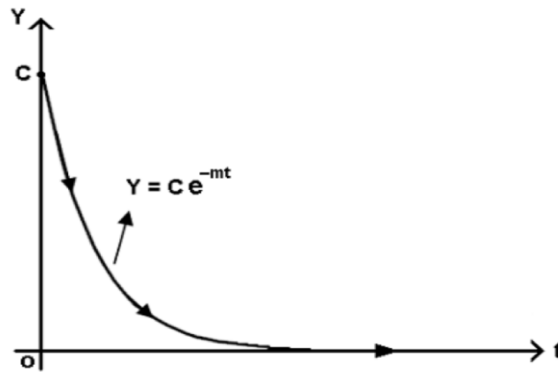


Figure 4.4. Exponential evolution path [86].

4.5.3. Analysis of Converter System

To synthesize the control law of the dynamic evolution controller, the dynamic equation of converter system must be analyzed and substituted into the dynamic evolution function (4.6).

The controlled converter which is presented in this research is the interleaved boost DC–DC converter. Since the interleaved boost converter works using two boost DC–DC converter in parallel, then the duty cycle analysis can be performed as a normal boost DC–DC converter.

Based on the state–space average model, the voltage and current dynamics of the boost DC–DC converter are given by,

$$v_{in} = L \frac{di_L}{dt} + V_o \cdot [1 - \alpha] \quad (4.7)$$

Where L is the inductance, C the capacitance, v_{in} the input voltage, i_L the inductor current, v_o the output voltage, and α the duty cycle, respectively.

Rearranging (4.7), the output voltage of the converter can be written as:

$$v_o = v_{in} + V_o \cdot \alpha - L \frac{di_L}{dt} \quad (4.8)$$

4.5.4. Synthesis of Duty Cycle Formula

The synthesis of duty cycle formula begins by defining the state error function (Y). The state error function is a linear of error voltage that defined as [87]:

$$Y = k \cdot v_{err} \quad (4.9)$$

where k is a positive coefficient, and v_{err} is error voltage.

$$v_{err} = V_{ref} - v_o \quad (4.10)$$

The derivative of (4.9) is given by:

$$\frac{dY}{dt} = k \cdot \frac{dv_{err}}{dt} \quad (4.11)$$

Substitution (4.9) and (4.11) into (4.6), yields

$$k \cdot \frac{dv_{err}}{dt} + (m \cdot k - 1) \cdot v_{err} + V_{ref} = v_o \quad (4.12)$$

Directly substituting the converter output voltage v_o from (4.8):

$$k \cdot \frac{dv_{err}}{dt} + (m \cdot k - 1) \cdot v_{err} + V_{ref} = v_i + v_o \cdot \alpha - L \frac{di_L}{dt} \quad (4.13)$$

Solving for α , the obtained duty cycle formula is given by:

$$\alpha = \frac{k \cdot \frac{dv_{err}}{dt} + (m \cdot k - 1) \cdot v_{err} + L \frac{di_L}{dt} + V_{ref} + -v_{in}}{v_o} \quad (4.14)$$

The expression for duty cycle α is the control action for the converter controller.

The state error function (Y) is forced to make evolution by following equation (4.15) and decrease to zero ($Y = 0$) with a decrease rate m . So, the state error function (Y) satisfy the error of e ,

$$Y = k \cdot v_{err} = 0 \quad (4.15)$$

Thus, the state error of the converter will converge to zero.

$$v_{err} = 0 \quad (4.16)$$

Substituting (4.10) into (4.17), the output voltage of converter during in the converters steady state [88]:

$$v_o = V_{ref} \quad (4.17)$$

From the synthesis procedure, the dynamic evolution controller works on the full nonlinear system and does not need any linearization or simplification on the system model at all as is necessary for application of traditional control theory.

The current control law from the above can be written as:

$$\alpha = \frac{V_{ref} - V_{in}}{v_o} + \frac{m.k - 1}{v_o} v_{err} + \frac{k}{v_o} \frac{dv_{err}}{dt} + \frac{L}{v_o} \frac{di_L}{dt} \quad (4.18)$$

It is interesting to note that the control law in (4.19) consists of four distinct parts. The first part is the feed-forward term $V_{ref} - v_{in}/v_o$, which is calculated based on the duty cycle. This term compensates for variations in input voltage. The second and third terms consist of proportional and derivative terms of the perturbations in the output voltage respectively. The last term consists of the derivative terms of the inductor current.

From (4.18), it is also seen that the input voltage, output voltage, and inductor current is involved in control output. The advantages are that the dynamic evolution control can compensate all of the variation in the input and output voltage and the change of inductor current. It contributes to the better dynamic performance of the controlled system.

4.5.5. PWM Duty Cycle Generation

The PWM duty cycle signals are generated by comparing a level control signal with a constant peak repetitive triangle signal (V_{st}). The frequency of the repetitive triangle signal establishes the switching frequency. This frequency is kept constant. Therefore, the dynamic evolution control is operated at the constant switching frequency.

Since the interleaved boost converter requires two PWM signals to drive both switches, additional work is necessary to generate two PWM signals from a single duty cycle formula. Figure 4.5 shows the PWM signal generation techniques [89]. The first PWM signal is produced when the control signal V_1 is less than V_{st} and the second PWM signal is produced when the control signal V_2 is greater than V_{st} .

The values of the desired level control signals are contracted from the calculation used the duty cycle formula, while the PWM signals are generated by (4.22).

$$v_1 = \alpha \quad (4.19)$$

$$v_2 = \overline{V_{ST}} - \alpha \quad (4.20)$$

$$\begin{aligned} PWM1 &= v_{st} > v_1 \\ PWM2 &= v_2 > v_{st} \end{aligned} \quad (4.21)$$

Where, V_{st} is the triangle signal and V_{ST} is the peak value of V_{st} .

The dynamic evolution control was proposed for interleaved boost DC–DC converter. The performance of the interleaved boost converter system under various duty cycle condition has been investigated.

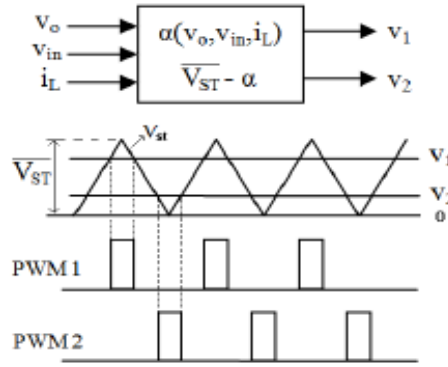


Figure 4.5. PWM signal generation [90].

4.6 Robust Adaptive Flatness Based Controller for Non-Ideal Boost Converter

From the controller design standpoint, boost converters exhibit the non–minimum phase phenomenon with the output voltage and current having different phase characteristics [91], and thus, developing a robust control strategy to assure tight reference voltage tracking under the condition of a wide range of input voltage variation and output load change is a challenging job. In this context, several researchers have proposed an effective solution. Namely, a multi–loop control approach whose core is transferring the outer voltage regulation problem into the inner current regulation problem. Based on this principle and according to the small signal model derived by conducting linearization around a nominal operating point from the state space average model, a dual loop proportional–integral (PI) control strategy, composed of an inner current loop and an outer

voltage loop, was successfully designed and applied to the DC–DC boost converter. However, due to the intrinsic nonlinearity of the switched converter and the operating point variation caused by unknown fluctuations on both the input voltage and the resistive load, the above linear control strategy is not able to respond well for a wide range of changes in operating points [92]. Thus, to obtain a favorable control performance for the nonlinear system, a controller with strong disturbance rejection capability and a fast dynamical response is required. Naturally, these demands force the consideration of nonlinear control algorithms which directly compensate for system nonlinearity without requiring a linear approximation.

In recent decades, many types of nonlinear controls have been proposed and applied to the DC–DC boost converters, such as sliding mode control, fuzzy logic control, and flatness based control. Among them, flatness based control, the earliest introduced in 1995, is an effective nonlinear control approach. A key merit of this control is that the profiles of the behavior of the nonlinear system can be well characterized by only the trajectories of a flat output and its derivatives. Additionally, the design parameters are independent of the operating point and easily selected [93]. As a result, with these features, a voltage loop with a flatness based controller will be adopted for the boost converter to enhance the system's performance in this paper.

Implementation of flatness based control is usually based on the power balance principle when applied to the outer voltage loop for DC–DC converters. Therefore, a precise knowledge of the Boost converter parameters like input voltage, load current and parasitic parameters should be effectively obtained. For the input voltage and the load current which may be subject to large uncertainties, the voltage sensor or the current sensor is generally used to measure these instantaneous values. However, the introduction of sensors will increase the implementation cost, while decreasing the control system reliability [94]. Therefore, under the condition without the use of sensors, several researchers have addressed the problem of uncertain input voltage and output load by utilizing adaptive law [95]. On the other hand, it is worth noticing that the parasitic parameters will cause power losses in the system.

If expecting a perfect tracking of the reference trajectory by the flat output, the converter losses should not be neglected. In this case, the author in [96] has pointed out that the converter losses can be modeled through two equivalent resistors (serial and parallel), and designed an online estimator to observe the values of the equivalent resistance. However, this estimation approach still needs to measure the input voltage and the load current. In fact, for flatness based control, serial and parallel resistances estimation can be transformed into the input voltage and the output current estimation respectively. In summary, the aforementioned problems can be addressed by designing a parameter adaption law which provides an online estimate of the unknown input voltage and the output current.

Hence, in this chapter, a robust adaptive flatness based control strategy for the voltage regulation loop of the non-ideal boost converter with an unknown input voltage and unknown output current is discussed. Meanwhile, because of clear functionality and ease of use, a PI controller is still applied to the inner loop for amending the inductor current. However, here, the focus is mainly made on the design of the adaptive flatness based control. The rest of this paper is organized as follows. In the section below, the equivalent circuit of non-ideal boost converter is presented and its mathematical model is established. Next, an adaptation law is derived based on state observers and an adaptive flatness based control is designed in detail in another section.

4.7 Modeling of Non-Ideal Boost Converter

In this part, a non-ideal boost converter which takes into account all types of parasitic parameters such as inductor series resistances, the on-resistance of conducting MOSFET transistors and diode forward voltages and resistance of the wire, is studied. Indeed, for easy analysis, from the viewpoint of the loss model, the total losses caused by those parasitic parameters can be divided into two parts which are presented by resistance in series with the input voltage source and by a resistance in parallel with the output load. Therefore, based on this principle, the model of a non-ideal boost converter is simplified and depicted in Figure 4.6 where the resistance in series and the resistance in parallel are noted by r_s and r_p , respectively. Following this, the equivalent state-space average model

of the non-ideal boost converter under continuous conduction mode (CCM) can be deduced as [97]:

$$\dot{x}_1 = -(1-u)\frac{x_2}{L} + \frac{V_{FC}}{L} - \frac{r_s}{L}x_1 \quad (4.22)$$

$$\dot{x}_2 = (1-u)\frac{x_1}{C} - \frac{1}{C}i_o \quad (4.23)$$

where the state variables x_1 and x_2 are the average inductor current i_L and the average capacitor voltage v_c , respectively. The parameters L and C represent the nominal values of the inductor and the capacitor, respectively and the control input u is the duty ratio. And the input voltage and the output current of the ideal boost converter are respectively denoted by V_{in} and i_o gave as follows:

$$V_{in} = V_{FC} - i_L r_s \quad (4.24)$$

$$i_o = \frac{v_c}{(R_o r_p / (R_o + r_p))} \quad (4.25)$$

Here, it is seen that, the value of V_{in} and i_o are unstable since the fuel cell V_{FC} , the equivalent series resistance r_s and the output resistance R may be subject to uncertain outer circumstances such as the power demands and temperature, etc. Therefore, to accurately acquire those uncertain values without the use of the sensors, the parameter adaption law b on observers can be designed.

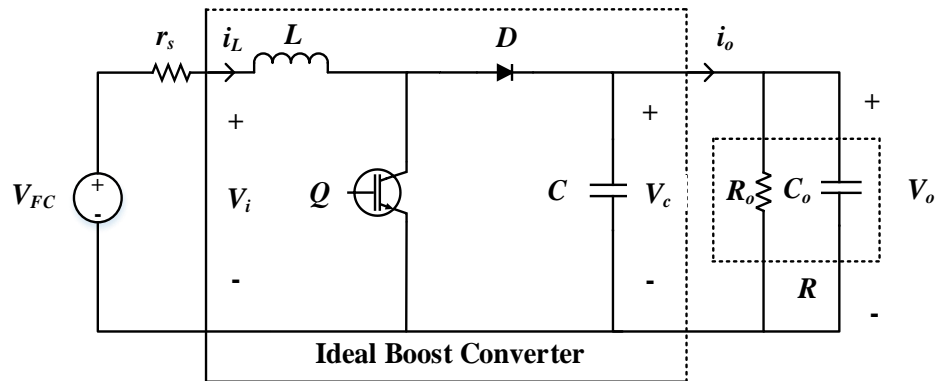


Figure 4.6. Equivalent circuit of non-ideal boost converter [98].

4.8 Controller Design of Non-Ideal Boost Converter

The objective of this section is to show how a dual loop control scheme comprising of an adaptive outer loop voltage controller looks like. This is done based on flatness-based control and an inner loop current controller based on PI control. A whole schematic block diagram of this control strategy is described in Figure 4.6. As clearly observed, reference voltage, despite unknown extern disturbance and the inner loops, is used to force the inductor current towards its reference current which is a slowly varying signal generated by the outer loop.

4.9 Sliding Mode Observer-Based Adaption Law Design

The input voltage V_{in} and the output current i_o of the boost converter are easily changed with the extern circumstances. Therefore, it is essential to follow their evolution to guarantee an effective output voltage control. Here, it is assumed that state variable x_1 and x_2 can be accessible. The state observers are designed as (4.26) and (4.27) to facilitate the design of parameter adaption laws for the boost converter [99].

$$\dot{\hat{x}}_1 = -(1-u)\frac{\hat{x}_2}{L} + \frac{\hat{V}_{in}}{L} + K_1 \text{sign}(x_1 - \hat{x}_1) \quad (4.26)$$

$$\dot{\hat{x}}_2 = -(1-u)\frac{\hat{x}_1}{C} - \frac{1}{C}\hat{i}_o - K_2 \text{sign}(x_2 - \hat{x}_2) \quad (4.27)$$

Where $K_1 > 0$ and $K_2 > 0$ are the observer gains, \hat{x}_1 and \hat{x}_2 are the estimate of x_1 and x_2 respectively while \hat{V}_{in} and \hat{i}_o are the estimates of V_{in} and i_o in that order.

Next, defining the estimation errors as follows:

$$\tilde{x}_1 = x_1 - \hat{x}_1, \tilde{x}_2 = x_2 - \hat{x}_2 \quad (4.28)$$

$$\tilde{V}_{in} = V_{in} - \hat{V}_{in}, \tilde{i}_o = i_o - \hat{i}_o \quad (4.29)$$

Then, using (4.26)–(4.29), we can obtain the following equations:

$$\dot{\tilde{x}}_1 = -(1-u)\frac{\tilde{x}_2}{L} + \frac{\tilde{V}_{in}}{L} + K_1 \text{sign}(\tilde{x}_1) \quad (4.30)$$

$$\dot{\tilde{x}}_2 = -(1-u)\frac{\tilde{x}_1}{C} - \frac{1}{C}\tilde{i}_o - K_2 \text{sign}(\tilde{x}_2) \quad (4.31)$$

To generate the adaption laws, the following function involving all estimation errors is chosen as:

$$V = \frac{1}{2}L\tilde{x}_1^2 + \frac{1}{2}C\tilde{x}_2^2 + \frac{1}{2\alpha_1}\tilde{V}_{in}^2 + \frac{1}{2\alpha_2}\tilde{i}_o^2 \quad (4.32)$$

where $\alpha_1 > 0$ and $\alpha_2 > 0$ are the adaption parameters for the designing.

The adaption laws are chosen as follows by the condition of $\dot{V} < 0$ is satisfied.

$$\dot{\hat{V}}_{in} = \alpha_1 \tilde{x}_1 \quad (4.33)$$

$$\dot{\hat{i}}_o = -\alpha_2 \tilde{x}_2 \quad (4.34)$$

Lastly, according to the LaSalle invariant principle, it can be concluded that $x_1 \rightarrow 0$ and $x_2 \rightarrow 0$ asymptotically. Thus, estimated parameters can be applied to flatness based controller design.

4.10 Adaptive Flatness Based Controller Design

After obtaining the estimation values of the unknown input voltage and the output current by the above analysis, an adaptive flatness based controller for the outer voltage loop can be derived. But before designing, it is necessary to prove whether the system is flat or not. In general, a system is said to be flat if and only is all system variable, namely state variable and the control vector, can be determined respectively from the flat outputs and their time derivatives. More precisely, without losing simplification [99].

$$\dot{x} = f(x, u), x \in R^n, u \in R^m \quad (4.35)$$

where $x = [x_1, x_2, \dots, x_n]^T$ and $u = [u_1, u_2, \dots, u_m]^T$ represent state vector and control vector respectively.

Next, if there exist a flat output vector $y \in R^m$ of the form:

$$y = (y_1, y_2, \dots, y_m) = \phi(x, u, \dot{u}, \dots, u^{(\alpha)}), \alpha \in N \quad (4.36)$$

$$\text{Such that, } \left\{ \begin{array}{l} x = \phi(y, \dot{y}, \dots, y^{(\beta)}) \\ u = \phi(y, \dot{y}, \dots, y^{(\beta+1)}) \end{array} \right\} \beta \in N \quad (4.37)$$

Based on the flatness control theory introduced above, one can choose the electrostatic energy as y stored in capacitor C as the flat output variable.

$$y = \frac{1}{2} C v_c^2 \quad (4.38)$$

From this, it is obvious that the state variable v_c , i.e. the voltage across the capacitor C , can be written as a function of the flat output.

$$v_c = \sqrt{\frac{2y}{C}} = \phi(y) \quad (4.39)$$

According to the non-ideal boost converter, by neglecting the electromagnetic energy in the inductor, the control variable P_L can be written as follows on basis of the power balanced principle.

$$P_L = \hat{V}_{in} \cdot \hat{i}_L = v_c \cdot \hat{i}_o = \phi\left(y, \dot{y}\right) \quad (4.40)$$

Clearly, the state variable v_c and the control variable P_L correspond to (4.39) in form. Consequently, the converter studied in this section can be considered as a flat system.

The desired energy reference for the capacitor is represented by y_{ref} . A linearizing feedback control law for ensuring reference tracking is given as follows [100].

$$(\dot{y} - \dot{y}_{ref}) + K_3(y - y_{ref}) + K_4 \int_0^t (y - y_{ref}) dt = 0 \quad (4.41)$$

Where K_3 and K_4 are the controller parameters chosen by analyzing the roots of the characteristics polynomial as follows:

$$p(s) = s^2 + K_3 s + K_4 = 0 \quad (4.42)$$

$$K_3 = 2\xi w_n, K_4 w_n^2 = 0 \quad (4.43)$$

Where ξ and w_n are the desired dominant damping ratio and the natural frequency, respectively. Clearly, based on the Routh–Hurwitz criterion law, the control system is stable when K_3 and K_4 are positive.

In addition, the inductor current reference I_{Lref} can be deduced by the following expression. Given that the outer loop is slower than the inner loop, the inductor current reference can be considered as a constant of small time interval.

$$I_{Lref} = \frac{P_L}{\hat{V}_{in}} \quad (4.44)$$

Finally, for the inner current loop, a simple PI controller can be utilized to guarantee the inductor current tracking and generate the switching control signal u .

$$u = K_p (L_{ref} - i_L) + K_i \int_0^t (L_{ref} - i_L) dt \quad (4.45)$$

Where K_p and K_i represent respectively the proportional gain and integral gain.

4.11 Superiority of Flatness Based Controller Design

For the non–ideal boost converter, this section has successfully shown a robust dual loop controller involving a novel adaptive flatness based control loop for voltage regulation as well as a simple PI control loop for the current tracking. The adaptation law is derived based on the state observer and Lyapunov function, thereby achieving an estimation for the input voltage and the output current of the ideal boost converter. In this way, the flatness

based control, in a combination of the adaptation law is designed and the proof of the stability is given by using Routh–Hurwitz criterion law. Compared with conventional flatness based control, the superiority of the adaptive flatness based control resides in not requiring the measurements of the input voltage and output current as well as estimation of the power losses.

4.12 Output Voltage Regulation of DC–DC Converter: Backstepping Control

In this chapter, the contribution of the fuel cell is used as a primary/main source controlled by the switches, for which an integral Backstepping–based nonlinear controller has been proposed.

4.13 Characteristics of DC–DC Converter over Linearity & Non-linearity

Characteristically, most DC–DC power converters are non-linear in nature, especially when the parasitic resistances are considered while modeling. The derivations in [101] clearly show that the averaged mathematical model of the DC–DC boost converter is nonlinear.

The authors in [102] used multi-input converter and designed a feedback proportional–integral controller by linearizing the system around the reference point using small-signal approximation. However, as discussed above, the DC–DC boost converter is itself, nonlinear. Therefore, using a linear approximation cannot give a stable solution over a wide operating range of the converter [103], and hence the global stability of the system is doubtful. Thus, the use of a nonlinear control scheme with a nonlinear mathematical model is the obvious choice [104]. There are, however, a few disadvantages, such as the nonlinear control scheme is computationally more complex and requires re-derivation each time there is a change in the mathematical model (such as an addition of another parasitic element in the model).

Using passive configuration of the DC bus, a Hysteresis based controller has been proposed for a battery–UC combination [105]. The resulting steady-state response is oscillatory because of its bounds being controlled manually. In [106], an FC–UC topology has been proposed where the stability of the system has been linked to an energy management system, making it a bit computationally costly.

A passivity-based nonlinear controller with an estimator using Fuzzy logic rules to decide the amount of UC current required instantaneously has been proposed in [107]. It performs observing the state of charge of UC and fuel in FC. However, the Fuzzy logic controller depends on a set of rules. The backstepping sliding mode control technique provides better results in terms of robustness [108].

The nonlinear backstepping control technique is recursive, and strict feedback from the model is needed for its design. Integral control is a basic control for the feedback system which can provide for parametric variations and slow time-varying external disturbances. The hybrid controller designed with the combination of integral control and conventional backstepping control technique provides greater robustness and removes steady-state error.

In this section, the integral of the tracking error ($e=x-x_d$) is added in the Lyapunov candidate function and the stability has been studied using Lyapunov based theory. The integral backstepping controller has been conferred to remove the steady-state error which the conventional backstepping controller has and performs far better than the Lyapunov Redesign based nonlinear controller as well.

4.14 FC Converter

A fuel cell (FC) uses hydrogen fuel to produce electricity. It has no carbon emissions and produces water as a by-product, hence it is extremely environmentally friendly. The type of FC used in this study is Proton Exchange Membrane Fuel Cell (PEMFC or simply FC) because of its compact size and low startup time. FC is different from a chemical battery in many aspects. It cannot be recharged conventionally and has a longer lifetime than battery. Therefore, a unidirectional DC-DC boost converter is used with an FC. This boost converter is used to step up the FC voltage to the required DC bus voltage (V_{dc}). It is also responsible for providing a steady and regulated DC bus voltage.

4.15 UC Converter

An ultra-capacitor (UC) stores charge electrostatically, and its electrical characteristics are very similar to a battery. However, it has some advantages over a battery: its charging and discharging rate (large power-density), greater count of life-cycles of a UC [109], and

large specific–power (though has small weight/size but can store a large amount of energy). As we know that a UC can be recharged by power obtained from regenerative braking and downhill motion, a bi–directional DC–DC buck–boost converter is connected with the UC. This converter acts as a boost converter when the power flows from UC to the DC bus (UC discharging) and it acts as a buck converter when the power flows from DC bus to the UC source (UC charging). It contains two switches S_1 & S_2 and one inductor L_2 with its internal resistance as depicted by R_2 .

4.16 Global Mathematical Model of FC: DC–DC Converter

The global mathematical–model of the FCEVs system is derived by [110],

$$\dot{x}_1 = -(1-u) \frac{x_3}{L_1} - \frac{R_1}{L_1} x_1 + \frac{V_{fc}}{L_1} \quad (4.46)$$

$$\dot{x}_2 = -U_{23} \frac{x_3}{L_2} - \frac{R_2}{L_2} x_2 + \frac{V_{uc}}{L_2} \quad (4.47)$$

$$\dot{x}_3 = (1-U_1) \frac{x_1}{C_o} + U_{23} \frac{x_2}{C_o} - \frac{I_o}{C_o} \quad (4.48)$$

For the state space model 1, the state variable/parameters and input parameters can be written as [111],

$$\begin{bmatrix} x_1 & x_2 & x_3 \end{bmatrix}^T = \begin{bmatrix} \langle i_{fc} \rangle & \langle i_{uc} \rangle & \langle v_{dc} \rangle \end{bmatrix}^T \quad (4.49)$$

$$\begin{bmatrix} U_1 & U_{23} \end{bmatrix}^T = \begin{bmatrix} \langle u_1 \rangle & \langle u_{23} \rangle \end{bmatrix}^T \quad (4.50)$$

Where, $\langle i_{fc} \rangle$ =average FC current, $\langle i_{uc} \rangle$ =average UC current, $\langle v_{dc} \rangle$ =average value of DC bus voltage, $\langle u_1 \rangle$ =average control input parameter u_1 , applied on the switch S_1 , $\langle u_{23} \rangle$ =average value of control input u_{23} . Here, the state variables of the system are taken by averaging the corresponding quantities in which the passive elements store energy, over one switching period. The control inputs are u_1 and u_2 which are the duty cycles of PWM applied to con the gates of MOSFET's switches of the buck–boost converter. Their values

lie in the interval $[0, 1]$. This model is nonlinear MIMO system; making the control design complex.

The control u_{23} has been defined as,

$$u_{23} = [(1 - K)u_3 + K(1 - u_2)] \quad (4.51)$$

Where, the control inputs u_2 and u_3 correspond to the switches S_2 and S_3 of the PWM respectively.

Also the buck and boost modes of the converter under consideration satisfy the following:

$$u_2 \in (0,1), u_3 = 0(off) \Rightarrow boost \quad (4.52)$$

$$u_2 = 0(off) u_3 \in (0,1) \Rightarrow buck \quad (4.53)$$

Note that when UC empowers DC bus, then $i_{uc} > 0$ and when it is recharged, regenerative, when vehicle is going slower, or during downhill motion, then $i_{uc} < 0$.

Now for I_{uc} being the reference of UC current, we define a variable K representing the mode of UC as follows: $K=1$ if $I_{uc} > 0$ and $K=0$ if $I_{uc} < 0$.

4.17 Design of Integral Backstepping Controller

The integral backstepping controller can be regulated using the DC bus voltage without having any steady-state error under load transients and variations. It is noted that FC continuously provides power to the load according to the demands of the system; finally, the stability of the system is also assured.

4.18 Indirect Current Control

The DC–DC boost converter exhibits a non–minimum phase response if the controller is used to track the v_{dc} voltage directly. Hence to avoid this problem, an indirect current control i_{fc} is defined. The current i_{fc} is selected since the FC source remains operational throughout the whole vehicle operational time and it only provides unidirectional power. Therefore, it is much easier to provide indirect current control using FC current i_{fc} . To achieve the indirect current control, the FC current reference, i_{fc} , is generated in such a way that i_{fc} is tracked to its reference by its controller. The DC bus voltage v_{dc} becomes equal

to its reference. The power equality equation is used to obtain the expression for the reference i_{fc} [118]

$$V_{fc}i_{fc} + V_{uc}i_{uc} = v_{dc}I_o \quad (4.54)$$

$$i_{fc}^{ref} = \lambda \left[\frac{v_{dc}I_o - V_{uc}I_o}{V_{fc}} \right] \quad (4.55)$$

Where, $\lambda > 1$ is the ideality factor that represents the losses in the power converters. Therefore, equation (4.55) shows the transformation of the voltage reference to the indirect current control reference.

First tracking error defined as:

$$z_1 = x_1 - x_{1ref} \quad (4.56)$$

The integral gain is given by:

$$\xi = \int_0^t (x_1 - x_{1ref}) dt \quad (4.57)$$

The integral term is defined by,

$$v_{z1} = \frac{1}{2} z_1^2 + \frac{\gamma}{2} \xi^2 \quad (4.58)$$

Since β is only a virtual control and the combined system will only be stabilized when defined an error:

$$z_2 = \frac{x_3}{L_1} - \beta \quad (4.59)$$

Using the composite function:

$$V_{zc} = V_{z1} + \frac{1}{2} z_2^2 \quad (4.60)$$

Here, $a_2 > 0$ and the composite candidate function becomes:

$$V_{zc} = -a_1 z_1^2 - a_2 z_2^2 \quad (4.61)$$

A control law using integral backstepping control which tracks FC current (i_{fc}) and the DC bus voltage (v_{dc}) to their respective desired values. It will continue to obtain a control law for track the UC up to the reference value of i_{uc} . Another error:

$$z_3 = x_2 - I_{sc}^{ref} \quad (4.62)$$

Taking the time derivatives of equation (4.62) and using the equation:

$$\dot{z}_3 = -u_{23} \frac{x_3}{L_2} - \frac{r_2}{L_2} x_2 + \frac{V_{sc}}{L_2} - I_{sc}^{ref} \quad (4.63)$$

Solving for u_{23} , the control law derived as [112]:

$$u_{23} = \frac{1}{x_3} \left[L_2 a_3 z_3 - r_2 x_2 + V_{sc} - L_2 I_{sc}^{ref} \right] \quad (4.64)$$

Here, a_3 is a positive constant. Hence, this is the final control law for the tacking of FC current obtained using integral backstepping technique.

The global asymptotic stability can be written as below:

$$V_{zc1} = -a_1 z_1^2 - a_2 z_2^2 - a_3 z_3^2 \quad (4.65)$$

The states of x_1 , x_2 and x_3 are supposed to be measurable without loss of generality. Therefore, designing an observer for the estimation of state variables is not part of the research. These state variables are voltages of the capacitors and the currents of the inductors which are measurable with the help of voltmeter and ammeter.

CHAPTER 5

Universal Sliding Mode DC–DC Converter Controller for Fuel Cell EV

5.1 Sliding Mode Controller for Quadratic Boost Converter

A fuel cell is a primary energy source and provides regular power to the propulsion system. Therefore, it is necessary to regulate the output voltage of FC. By way of, the voltage profile of FC is less, a quadratic boost converter to maintain DC bus voltage in proportion to load change. This section presents a quadratic boost converter for boosting the voltage profile in load change condition and for controlling the voltage profile of DC bus by using a sliding mode controller.

5.2 Power Management System of FC: Quadratic Converter

A quadratic boost converter is interfaced in FC and DC bus. Input control management for FC is extremely necessary as load changes. The input of FC is controlled with the assistance of a PI controller as shown in Figure 5.1.

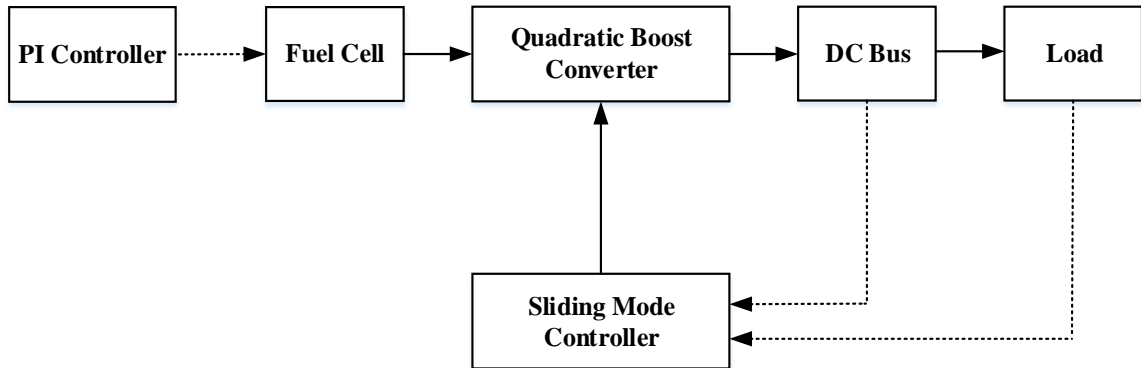


Figure 5.1. Power management of FC [113].

The desired value of the fuel cell is regulating the input of the fuel cell (hydrogen and air) with the help of the PI controller. This PI controller controls the amount of hydrogen and air according to the desired fuel cell current. The sliding mode controller controls the output voltage of the quadratic boost converter at the DC bus during transient condition or variation in load demand.

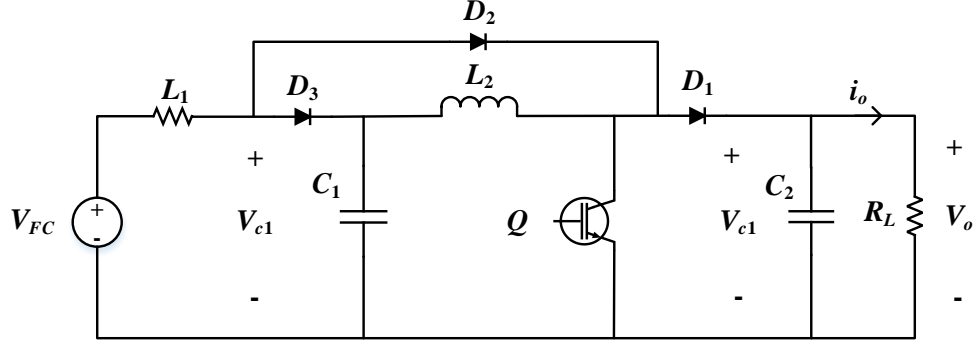


Figure 5.2. Model of quadratic boost converter [114].

5.3 Modeling of Quadratic Boost Converter

Caused by limited switching frequency of the conventional boost converter, components of two conventional boost converters are combined such as a single switch can control the complete system which will improve the voltage profile of the DC bus and improves the switching frequency of converter.

Order of quadratic boost converter is for having two commutation cells which run at the same time. Combination of semiconductor controlled switch (IGBT and MOSFET) Q and semiconductor diode D_1 forms initial cell, which forms a step-up chopper, inductor L_2 and capacitor C_2 . The second cell having semiconductor diodes D_3 and D_1 .

For continuous mode operation of quadratic boost converter; semiconductor switch S and semiconductor diode D_2 will conduct, and semiconductor diodes D_1 and D_3 are not conducting during ON-state. In the case of OFF-state condition, semiconductor switch Q and semiconductor diode D_2 are not conducting. Additionally, in this state semiconductor diode, D_1 and D_3 are conducting.

The differential equation for each converter state can be reformed as bilinear model [115].

$$\frac{di_{L1}}{dt} = \frac{v_i}{L_1} - \frac{v_{c1}}{L_1} (1 - u) \quad (5.1)$$

The control variable u is used for controlling switch S applied for gate, if $u=1$ then it will work for ON-state and if $u=0$ then it will work for OFF-state

By putting the value of u in equation 5.1 the average value of u is representing by duty cycle D . The transfer function of the quadratic boost converter at ideal and the steady-state condition represents by the equation below [116].

$$\frac{v_{c1}}{v_i} = \frac{v_{c2}}{v_{c1}} = \frac{1}{1-D} \quad (5.2)$$

$$M(D) = \left(\frac{v_{c2}}{v_{c1}} \right) \left(\frac{v_{c1}}{v_i} \right) = \frac{1}{(1-D)^2} \quad (5.3)$$

During load variation, since the voltage drops in output, it is necessary to regulate this voltage with the help of a close loop feedback system.

Voltage regulation of the quadratic boost converter at DC bus can be regulated by two loop management methods. These are known as the inner loop and outer loop. The function of the inner loop is to regulate the inductor (L_1) current. The function of the outer loop provides the reference current for the inner loop which is the error of output voltage [117]. The switching of the converter is done by a hysteresis band based system [118]. The inner current loop introduces the sliding surface $S(x)$ and operates the converter at a stable point. The function of outer loop is to generate reference current I_E for the inner loop and to regulate the output voltage of the quadratic boost converter at DC bus during transient conditions. The dynamic response of $I_E(t)$ is slow as compared to input inductor current so therefore it is easy to an analysis of both the loop.

5.4 Controller for the Circuit Analysis (Sliding Mode Controller)

The control technique is formed based on the sliding surface; it can be defined using the inductor current of input.

$$S(x) = i_{L1} - I_E(t) \quad (5.4)$$

Where $I_E(t)$ can be given as [119],

$$I_E(t) = -K_p (v_{c2}(t) - V_{ref}) - K_i \int_{-\infty}^t (v_{c2}(\lambda) - V_{ref}) d\lambda \quad (5.5)$$

The switch function tends to sliding motions expressed as follows:

Here, $\mu=1$ when switch is ON and $\mu=0$ during the switch OFF Period.

Estimating the reality condition $S(x)$. $S(x)<0$ with the help of control law leads to the local reach ability condition [120].

$$0 < v_i - L_1 \frac{dI_E}{dt} < v_{c1} \quad (5.6)$$

By applying $S(x)=0$ and $S(x)=0$ in (5.1–5.6) the equivalent control signal is given by (5.7).

$$u_{eq} = 1 - \frac{1}{v_{c1}} (v_i - L_1 \frac{dI_E}{dt}) \quad (5.7)$$

When equation of the equivalent control and $S(x) = 0$ is introduced in (5.1), resulting ideal sliding dynamics of the converter.

$$\frac{dv_{c2}}{dt} = -\frac{v_{c2}}{RC_2} + \frac{i_{L2}}{C_2} \frac{1}{v_{c1}} \left(v_i - L_1 \frac{dI_E}{dt} \right) - \frac{i_o}{C_2} \quad (5.8)$$

Finding the equilibrium point of (5.8), considering that $i_E(t)$ has constant value I_E , expression (5.9) can be obtained.

$$\bar{v}_{c1} = (I_E R)^{\frac{1}{4}} v_i^{\frac{3}{4}}; \bar{v}_{c2} = (I_E v_i R)^{\frac{1}{2}} \quad (5.9)$$

$$\bar{i}_{L1} = I_E; \bar{i}_{L2} = I^{\frac{3}{4}} E \left(\frac{v_i}{R} \right)^{\frac{1}{4}} \quad (5.10)$$

After linearizing the (5.10) at equilibrium point obtained from (5.8), the equation (5.9) can be written as (5.11).

$$\frac{di_{L2}}{dt} = \frac{2\tilde{v}_{c1}}{L_2} - \frac{\tilde{v}_i}{L_2 \bar{v}_{c1}} \bar{v}_{c2} + \frac{L_1 \bar{v}_{c2}}{L_2 \bar{v}_{c1}} \frac{d\tilde{i}_E}{dt} - \frac{\bar{v}_{c2}}{L_2 \bar{v}_{c1}} \tilde{v}_i \quad (5.11)$$

$$\frac{d\tilde{v}_{c1}}{dt} = -\frac{1}{C_1} \tilde{i}_{L2} - \frac{\bar{i}_E}{C_1 \bar{v}_{c2}} \tilde{v}_{c1} + \frac{\tilde{v}_i}{C_1 \bar{v}_{c1}} \bar{i}_E - \frac{L_1 \bar{i}_E}{C_1 \bar{v}_{c1}} \frac{d\tilde{i}_E}{dt} + \frac{\bar{i}_E}{C_1 \bar{v}_{c1}} \tilde{v}_i \quad (5.12)$$

$$\frac{d\tilde{v}_{c2}}{dt} = \frac{\tilde{v}_i}{C_2 \bar{v}_{c1}} \tilde{i}_{L2} - \frac{\tilde{i}_{L2}}{C_2 \bar{v}_{c2}} \tilde{v}_{c1} - \frac{1}{RC_2} \tilde{v}_{c2} - \frac{L_1 \tilde{i}_{L2}}{C_2 \bar{v}_{c1}} \frac{d\tilde{i}_E}{dt} + \frac{\tilde{i}_{L2}}{C_2 \bar{v}_{c1}} \tilde{v}_i - \frac{1}{C_2} \tilde{i}_o \quad (5.13)$$

Where, the superscript (\sim) stands for the increments of variable in (5.12).

Applying Laplace transformation to (5.13), functions (5.14)–(5.18) can be obtained. Where $V_{c2}(S)$ is output of linearized system, $I_E(S)$ is the respective input, and $I_o(S)$ and $V_i(S)$ represents an output load variation and an input voltage perturbation, respectively. The terms $A(s)$, $B(s)$, $C(s)$ and $D(s)$ is shown in equation below [121]:

$$A(s)V_{c2}(s) = B(s)I_E(s) + C(s)V_i(s) - D(s)I_o(s) \quad (5.14)$$

$$A(s) = L_2 C_2 \bar{v}_{c2} s^3 + T_{L2} \bar{v}_{c2} \left(K_m^2 \frac{C_2}{C_1} + 1 \right) s^2 + \left[\bar{v}_{c2} \left(K_m^2 \frac{T_{L2}}{T_{c1}} + 2 \frac{C_2}{C_1} \right) + \bar{v}_i \right] s + 4 \frac{\bar{v}_{c2}}{T_{c1}} \quad (5.15)$$

$$B(s) = K_m^2 T_{L1} T_{L2} R \bar{v}_{c2} s^3 + T_{L1} R \bar{v}_{c2} s^2 + \left[\frac{K_m^2 R}{T_{c1}} \left(2 T_{L1} \bar{V}_{c2} + T_{L2} \bar{v}_i \right) \right] s + \frac{2 R \bar{v}_i}{T_{c1}} \quad (5.16)$$

$$C(s) = K_m^2 T_{L2} \bar{v}_{c2} s^2 - \bar{v}_{c2} s + 2 \frac{K_m^2 \bar{v}_{c2}}{T_{c1}} \quad (5.17)$$

$$D(s) = T_{L2} R \bar{v}_{c2} s^2 + \frac{K_m^2 T_{L2} R \bar{v}_{c2}}{T_{c1}} s + \frac{2 R \bar{v}_{c2}}{T_{c1}} \quad (5.18)$$

Where, superscript ($-$) shows the equilibrium values of the state variables. Thus, the transfer function from the incremental input current to the incremental output voltage could be obtained by neutralizing the dynamic behavior of both disturbances.

$$G_i(s) = \frac{V_{c2}(s)}{I_E(s)} = \frac{B(s)}{A(s)} \quad (5.19)$$

$$G_o(s) = \frac{V_{c2}(s)}{I_o(s)} = \frac{D(s)}{A(s)} \quad (5.20)$$

Transfer function of the PI compensation in the outer loop is stated in the below equation,

$$G_e(s) = K_p + \frac{Ki}{s} \quad (5.21)$$

The closed-loop transfer function of desired voltage to actual voltage at the DC bus given by (5.22),

$$G_{vo}(s) = \frac{G_e(s)B(s)}{A(s) + G_e(s)B(s)} \quad (5.22)$$

Therefore, the equation will be given by [[122],

$$P(s) = s[A(s) + G_e(s)B(s)] \quad (5.23)$$

$$P(s) = p_4s^4 + p_3s^3 + p_2s^2 + p_1s + p_0 \quad (5.24)$$

$$p_0 > 0, p_1 > 0, p_2 > 0, p_3 > 0, p_4 > 0 \quad (5.25)$$

$$p_1 = a_0 + b_1K_i + b_oK_p \quad p_0 = b_oK_i \quad (5.26)$$

$$p_2 = a_1 + b_2K_i + b_1K_p \quad (5.27)$$

$$p_3 = a_2 + b_3K_i + b_2K_p \quad (5.28)$$

$$p_4 = a_3 + b_3K_p \quad (5.29)$$

$$p_2p_3 - p_1p_4 > 0, p_1p_2p_3 - p_1^2p_4 - p_0p_3^2 > 0 \quad (5.30)$$

For each value of p_0, p_1, p_2, p_3 and p_4 ; the equation (5.30) must be satisfied for stable operation of the system.

The objectives of this controller model are to fulfill the required constant voltage at the transient condition of the system. Consequently, the DC bus or load voltage, load current and load power can be obtained by the system parameter variation.

5.5 Sliding Mode Controller Based Interleaved Boost Converter for Fuel Cell System

When two conventional boost converter are connected in parallel these arrangements of the conventional boost converter are known as interleaved boost converter (IBC) [123]. Parallel connection of boost converter usually shares high input current, interleaving is the most suitable process for high power applications, such as fuel cell electric vehicle. Additionally, interleaving is the most suitable converter for boosting voltage profile of fuel cell in EV.

Therefore, a suitable controller is necessary to control the output DC-bus voltage of IBC. The nature of step-up chopper is non-linear time-varying, that's why it is necessary to fulfill the above property of the system by designing controller appropriately

5.6 Modeling Strategy of Interleaved Boost Converter

Interleaved boost converter (IBC) is used to tackle high current problems with high power applications.

In this section, continuous conduction mode is explained. Converters components are taken equal values for making mathematics simple. So $L_1=L_2=L$ and duty cycle of switch S_1 and S_2 is taken. The continues conduction mode is explained as follows [124].

1) State a

S_1 is switched on and switch S_2 is switched off. Inductor current of L_1 start to increase and inductor current of L_2 start to decrease. Inductor current change rate for L_1 is $diL_1/dt=V_{fc}/L$, and for inductor L_2 is $diL_2/dt=(V_{fc}-V_o)/L$

2) State b

S_1 and S_2 both will remain in off condition; both inductor current I_{L1} and I_{L2} will discharge through load. At this condition, the change rate for inductor current are given below, made $diL_1/dt=diL_2/dt=(V_{fc}-V_o)/L$.

3) State c

S_2 will be on condition while S_1 will continue in off condition, inductor current of L_1 continue to discharge. Inductor current change rate of L_2 is given by $diL_2/dt=V_{fc}/L$ and $diL_1/dt=(V_{fc}-V_o)/L$

4) State d

S_2 is off and S_1 is still open, inductor L_1 and L_2 discharge through load. For this state, $diL_1/dt=diL_2/dt=(V_{fc}-V_o)/L$.

5.7 Interleaved Converter System Analysis

As controlled converter used for this research is IBC which is combination of two parallel connected conventional boost converters, then duty cycle analysis of interleaved boost converter can also be analyzed as conventional boost DC–DC converter.

$$\frac{di_L}{dt} = -(1-u) \frac{V_o}{L} + \frac{V_{fc}}{L} \quad (5.31)$$

$$\frac{dV_c}{dt} = (1-u) \frac{i_L}{C} - \frac{V_c}{RC} \quad (5.32)$$

Let $I_L = X_1$ and $V_o = X_2$, the state space–equation given by [125],

$$\dot{x}_1 = -(1-u) \frac{x_2}{L} + \frac{V_{fc}}{L} \quad (5.33)$$

$$\dot{x}_2 = (1-u) \frac{x_1}{C} - \frac{1}{RC} x_2 \quad (5.34)$$

$$\begin{bmatrix} \dot{x}_1 \\ \dot{x}_2 \end{bmatrix} = \begin{bmatrix} 0 & -\frac{1}{L} \\ \frac{1}{C} & -\frac{1}{RC} \end{bmatrix} \begin{bmatrix} x_1 \\ x_2 \end{bmatrix} + \begin{bmatrix} \frac{V_{fc}}{L} \\ -\frac{x_2}{C} \end{bmatrix} \quad (5.35)$$

When V_{fc} , V_o and I_L fuel cell voltage, load voltage and input or inductor current respectively. Due to load variation inductor current never falls to zero in continuous mode.

5.8 Methodology of Sliding Mode Controller

The surface of sliding is a force trajectory which follows the system to establish a path in the state variable space; a high speed switching control law, that may be used is called the variable structure controller (VSC).

Control objective of sliding mode controller is to validate the following condition [126]:

$$\lim_{t \rightarrow \infty} V(c) = V_r \quad (5.36)$$

The reference output voltage is defined as V_r . System parameters and unforeseen disturbance in boost converter does not affect performance of controller.

A sliding surface should be there to determine the sliding motion for a sliding mode controller (SMC). For this persistence, sliding surface is defined in equation (5.37).

$$S(x) = K_1(x_1 - I_r) + (K_2 - V_r) \quad (5.37)$$

Here, K_1 and K_2 is represented by sliding surface constant. I_r and V_r is reference input and reference voltage at DC-bus or load respectively.

Sliding mode will be there when,

$$S(x) = \dot{S}(x) = 0 \quad (5.38)$$

The generalized control structure u is combination of u_n and equivalent control component u_{eq} .

$$u = u_n + u_{eq} \quad (5.39)$$

Where, u_{eq} can be given as (5.40) [126],

$$u_{eq} = \left[\frac{\partial S}{\partial x} B(x) \right]^{-1} \left(\frac{\partial S}{\partial x} A(x) \right) \quad (5.40)$$

Differentiating equation (5.40) in with to x then,

$$\frac{\partial S}{\partial x} [K_1 \ K_2] \quad (5.41)$$

$$\left(\frac{\partial S}{\partial x} B(x) \right)^{-1} = \frac{LC}{[(K_1 C x_2 - K_2 L x_1)]} \quad (5.42)$$

$$\frac{\partial S}{\partial x} A(x) = \frac{-K_1 R C x_2 LC + K_2 L (K_1 R - x_2 C)}{RLC} \quad (5.43)$$

By putting equation (5.41), (5.42) in (5.43) possible to get u_{eq} as,

$$u_{eq} = \left[\frac{-K_1 R C x_2 LC + K_2 L (k_1 R - x_2 C)}{K_1 x_2 RC - K_2 x_1 RL} \right] \quad (5.44)$$

Similarly,

$$u_n = K_3 \text{sign}(S(x)) \quad (5.45)$$

Controlling signal can be obtained by putting the value of u_{eq} and u_n in equation (5.46),

$$u = \left[\frac{-K_1 R C x_2 LC + K_2 L (k_1 R - x_2 C)}{K_1 x_2 RC - K_2 x_1 RL} \right] + k_3 \text{sign}(S(x)) \quad (5.46)$$

Equation (5.46) is used to generate the controlling signal for switch S_1 and S_2 with the help of pulse width modulation (PWM).

5.9 Duty Cycle Generation of PWM

The control signal u , along with the carrier signal especially, forms triangle PWM duty cycle. The switching frequency of semiconductor switches S_1 and S_2 are equal to the frequency of carrier signal. An interleaved boost converter has two semiconductor switches. Therefore, the PWM signal is required for driving both switches S_1 and S_2 [127]. First PWM signal (G_1) is generated when the peak of the control signal (u) is lesser than the peak of a carrier signal, and second PWM signal (G_2) is generated when the peak of control is greater than the peak of a carrier signal

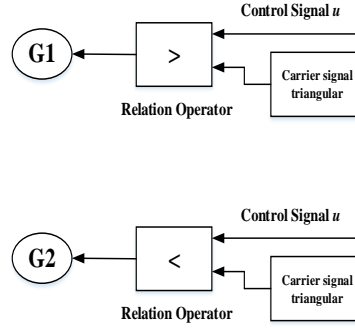


Figure 5.3. PWM duty cycle generation [128].

5.10 Sliding Mode Control: Cascade Boost Converter for Fuel Cell Energy Generation System

The FCs have nonlinear and non-regulated DC output power so they need interfaced system to have suitable levels of input and output voltage. Doing so ensures the FCs and the load are both kept safe.

In this section, the system interface used is a DC–DC cascade boost converter that steps up the low output voltage. Conventional DC–DC cascade boost converter has a wider voltage ratio. However, power losses increase by connecting additional conventional DC–DC boost converter in a cascade is found from [129]. The DC–DC cascade boost converter, which has a different topology, uses only a switch and has a quadratic duty cycle. The control method used for DC–DC cascade boost converter must overcome its nonlinearity and variation of voltage to provide stability for all conditions with fast response.

This discussion is mainly focused on the control of DC–DC cascaded boost converter associated to the main FC source.

Based on the nonlinear model of the whole system, a sliding mode controller (SMC) can be elaborated to regulate the output voltage to ensure the asymptotic stability of the closed-loop system.

5.11 DC–DC Cascade Boost Converter Model

The DC–DC cascade boost converter circuit has a high boost rate with a low duty cycle, the low voltage stress on components, and high efficiency [130]. These features allow the DC–DC cascade to boost converter circuit to be more favorable than the conventional DC–

DC boost converters. The DC–DC cascade boost converter consists of one switch, two boost inductors L_1 and L_2 , three diodes D_o , D_1 and D_2 and capacitors C_1 and C_o

The DC–DC cascade boost converter, which is connected to PEMFC, is derived from the conventional DC–DC boost converter topology by adding L_2 , D_o , D_2 , and C_o . This circuit is built by only one active switch. DC–DC cascade boost converter, that uses only a switch M in Figure 5.4 is shown where; V_{in} is the input voltage of the circuit, the MOSFET that is used for switching of M , D_1 , D_2 and D_o are diodes that work as passive switch, L_1 and L_2 are the inductances, C_1 and C_o are capacitances. V_o is the output voltage of the converter. The DC–DC cascade boost converter. The first conventional DC–DC boost converter consists of L_1 , D_1 , D_2 , C_1 , M (switch). M is at ON position, so C_1 capacitor is charged to V_{c1} with,

$$\frac{V_{c1}}{V_{in}} = \frac{1}{1-\mu} \quad (5.47)$$

The second conventional DC–DC boost converter consists of C_1 , L_2 , M , D_o , and C_o . The voltage transfer gain of this circuit given by,

$$\frac{V_o}{V_{c1}} = \frac{1}{1-\mu} \quad (5.48)$$

The total voltage transfers gain of DC–DC cascade boost converter is then obtained as follows,

$$\frac{V_o}{V_{in}} = \frac{1}{(1-\mu)^2} \quad (5.49)$$

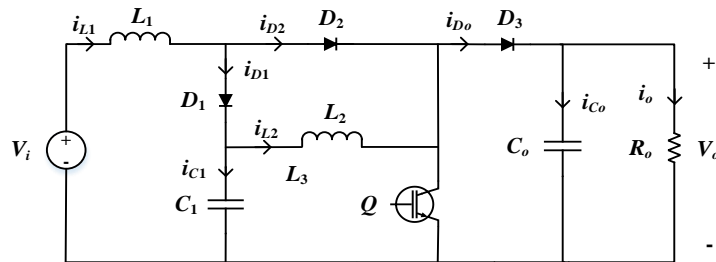


Figure 5.4. DC–DC cascade boost converter [131].

From the investigation of modeling the DC–DC cascade boost converter; it can be shown that the converter topology changes according to M switch ON and OFF positions. Using Kirchhoff's law and averaging technique, the following state space averaged model is obtained as [132],

$$\frac{dx_1}{dt} = -\frac{(1-\mu)}{L_1}x_3 + \frac{1}{L_1}V_{in} \quad (5.50)$$

$$\frac{dx_2}{dt} = -\frac{(1-\mu)}{L_2}x_4 + \frac{1}{L_2}V_{x3} \quad (5.51)$$

$$\frac{dx_3}{dt} = -\frac{(1-\mu)}{C_1}x_1 - \frac{1}{C_1}x_2 \quad (5.52)$$

$$\frac{dx_4}{dt} = -\frac{(1-\mu)}{C_o}x_2 - \frac{1}{C_o R_o}x_4 \quad (5.53)$$

Where, x_1 x_2 x_3 and x_4 denote the averaged values, respectively of the first inductor current i_{L1} , the second inductor current i_{L2} , the capacitor voltage v_{c1} and the output voltage v_o . The signal μ is a duty ratio which acts as the control input of the system. The model of (5.50)–(5.53) are bilinear which makes the control problem a difficult job.

5.12 Sliding Mode Controller Analysis [133]

The control objectives are to regulate the output capacitor voltage v_o to a desired constant value V_d to take into account the nonlinear behavior of the FC and DC–DC cascade boost. To this end, the sliding mode control (SMC) approach is accepted [134]. First, the equilibrium points must be determined by letting the right side of (5.54)–(5.57) equal to zero.

$$x_{10} = \frac{V_d^2}{V_{in} R_o} \quad (5.54)$$

$$x_{20} = \frac{1}{R_o} \sqrt{\frac{V_d^3}{V_{in} R_o}} \quad (5.55)$$

$$x_{30} = \sqrt{V_{in} V_d} \quad (5.56)$$

$$x_{40} = V_d \quad (5.57)$$

To define the following state vector $x = [x_1, x_2, x_3, x_4]^T$, equations (5.54)–(5.57) can be written in the following compact [134]:

$$\dot{x} = Ax + g(x)\mu + f_o \quad (5.58)$$

$$\text{Where, } A = \begin{pmatrix} 0 & 0 & -\frac{1}{L_1} & 0 \\ 0 & 0 & \frac{1}{L_o} & -\frac{1}{L_2} \\ \frac{1}{C} & -\frac{1}{C_1} & 0 & 0 \\ 0 & \frac{1}{C_o} & 0 & -\frac{1}{C_o R_o} \end{pmatrix} \quad (5.59)$$

$$g(x) = \begin{pmatrix} \frac{x_3}{L_1} \\ \frac{x_4}{L_2} \\ -\frac{x_1}{C_1} \\ -\frac{x_2}{C_o} \end{pmatrix} \quad f_o = \begin{pmatrix} \frac{V_{in}}{L_1} \\ \frac{x_4}{L_2} \\ -\frac{x_1}{C_1} \\ -\frac{x_2}{C_o} \end{pmatrix} \quad (5.60)$$

It is known that the SMC provides a method to design a system in such a way that the controlled system is insensitive to parameter variations and external load disturbances. The main objective of the SMC is to make the system evolve on a surface containing the desired equilibrium point. Such an equilibrium point must be an asymptotically stable point of the system's trajectory restricted to the surface. Several sliding surfaces are presented and studied. However, by taking into account the control objectives and the fact that the cascade boost converter has a no-minimum phase features, from where the following sliding surface can be,

$$S = K_1 e_1 + K_2 e_2 + K_3 e_3 + K_4 e_4 \quad (5.61)$$

The errors are given by [135],

$$e_1 = x_1 - x_{10} \quad (5.62)$$

$$e_2 = x_2 - x_{20} \quad (5.63)$$

$$e_3 = x_3 - x_{30} \quad (5.64)$$

$$e_4 = x_4 - x_{40} \quad (5.65)$$

Where k_1, k_2, k_3 and k_4 are the design parameters.

The derivatives of the sliding surface along the trajectories (5.62)–(5.65) can be obtained as follows,

$$\dot{S} = \frac{ds}{dt} = \frac{\partial S}{\partial x} \left(\frac{\partial S}{\partial t} \right) = \frac{\partial S}{\partial x} \dot{x} \quad (5.66)$$

Which using (5.66), yields,

$$\dot{S} = \frac{\partial S}{\partial x} (Ax + g(x) \cdot \mu + f_o) \quad (5.67)$$

The control law of μ is composed by two components. An equivalent component μ_{eq} and a nonlinear component μ_N ,

$$\mu = \mu_{eq} + \mu_N \quad (5.68)$$

The equivalent control component constitutes a control unit when exciting the motion of the system on the sliding surface. However, the second component μ_N is to ensure the equilibrium $S=0$ to be globally asymptotically stable.

The equivalent control is obtained as the solution of [135],

$$\dot{S} = \frac{\partial S}{\partial x} (Ax + g(x) \cdot \mu_{eq} + f_o) = 0 \quad (5.69)$$

$$\mu_{eq} = \left[\frac{\partial S}{\partial x} g(x) \right]^{-1} \left\{ \frac{\partial S}{\partial x} (Ax + f_o) \right\} \quad (5.70)$$

Where,

$$\frac{\partial S}{\partial x} g(x) = \frac{K_1}{L_1} x_3 + \frac{K_2}{L_2} x_4 - \frac{K_3}{C_1} x_1 - \frac{K_4 x_2}{C_o} \quad (5.71)$$

$$\frac{\partial S}{\partial x} g(x) \neq 0, \partial t > 0 \quad (5.72)$$

$$\frac{\partial S}{\partial x} (Ax + f_o) = (k_1 \ k_2 \ k_3 \ k_4) \begin{pmatrix} -\frac{1}{L_1} x_3 + \frac{1}{L_1} V_{in} \\ \frac{1}{L_2} x_3 - \frac{1}{L_2} x_4 \\ \frac{1}{C_1} x_1 - \frac{1}{C_1} x_2 \\ \frac{1}{C_o} x_2 - \frac{1}{C_o R_o} x_4 \end{pmatrix} \quad (5.73)$$

The nonlinear component will be determined to ensure the attractiveness of the controlled trajectory toward the sliding surface. The nonlinear control component can be chosen as follows [136]:

$$\mu_N = \left[\frac{\partial S}{\partial x} g(x) \right]^{-1} \hat{\mu}_N \quad (5.74)$$

It is also required to satisfy the condition of the convergence.

$$S \dot{S} < 0 \quad (5.75)$$

For a sliding mode to exist, the state vector x should be driven to reach the sliding surface and afterwards be constrained to this surface. That is, the surface must be rendered attractive and invariant by an appropriate switching of the control μ .

$$V(x) = \frac{1}{2} S^2 \quad (5.76)$$

The time derivative is,

$$\dot{V} = S \dot{S} \quad (5.77)$$

The derivatives of the sliding surface can be written follows [136]:

$$\dot{S} = \frac{\partial S}{\partial x} Ax + \left(\frac{\partial S}{\partial x} g(x) \right) \left[\mu_{eq} + \left(\frac{\partial S}{\partial x} g(x) \right)^{-1} \hat{\mu}_N \right] + f_o \quad (5.78)$$

That leads to,

$$\dot{S} = \hat{\mu}_N \quad (5.79)$$

The derivative of the function can be written as follows,

$$\hat{\mu}_N = -\lambda S \quad (5.80)$$

Indeed, with this (5.80) becomes,

$$\dot{V} = -\lambda S^2 \quad (5.81)$$

This is clearly ensuring that the equilibrium $S=0$ is globally asymptotically stable [137].

Finally combining (5.78)– (5.81) the following sliding mode controller universal law is obtained:

$$\mu = - \left[\frac{\partial S}{\partial x} g(x) \right]^{-1} \left\{ \left[\frac{\partial S}{\partial x} (Ax + f_o) - \lambda S \right] \right\} \quad (5.82)$$

5.13 Simulation Results

In Figure 5.5, the dual PEMFC fuel cell stack is used to ensure the efficiency is around 95%. Where, both of the fuel cell stack are connected by bus selector to represent the voltage, current and efficiency of the FCEV.

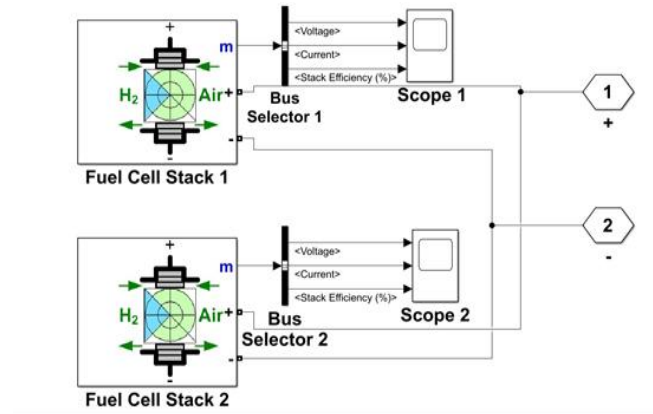


Figure 5.5. The selection of fuel cell stack.

In this section, the system is simulated and the performance of the SMC has been investigated as shown in Figure 5.6. The main objectives of the controller are to maintain the constant desired output voltage at the DC bus during the transient condition and to regulate the power depending on the operating condition.

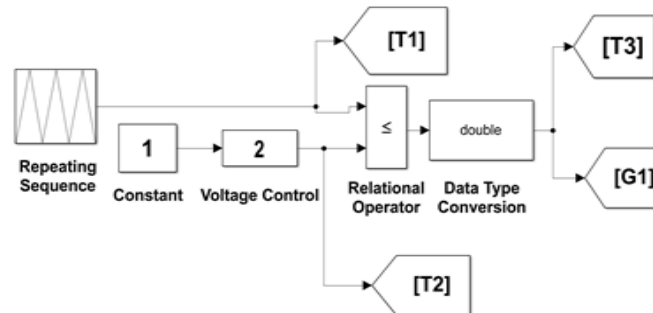


Figure 5.6. Voltage controller of SMC DC-DC converter.

During the starting condition, usually the FC cannot provide instant power. However, by using SMC, the FC is able to supply the load demand by maintaining the rated voltage and current along with the rated stack efficiency based on the DC bus voltage requirement of the electric vehicle (Figure 5.7). Additionally, it is apparent that the current has a low rise time and is able to reach stability quickly. This rise time is approximately 0.005 s. The stack efficiency is stable throughout the simulation as well. The voltage initially decreases from approximately 800 V to 600 V at the start of the simulation as well. However, the voltage is able to become stable and continues to be 600 V for the majority of the experiment.

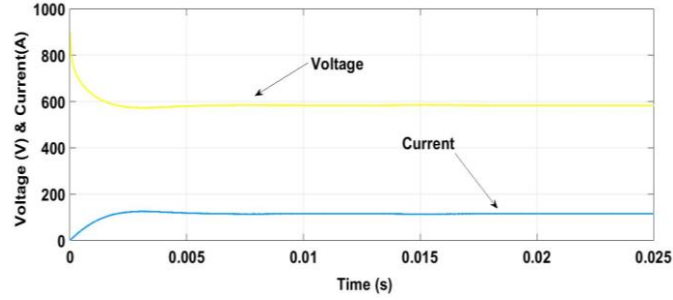


Figure 5.7. V-I Characteristics of DC-DC converter for FCEV.

It is possible to boost up the load voltage significantly. This increased the overall power rating more times higher as noted on Figure 5.8. It is also clear that, voltage with stabilized peak point ensures a small amount of harmonics even with lower time derivatives. Furthermore, it is clear within Figure 5.8 that two harmonics are present and the output voltage stabilizes at approximately 0.005 s at 900 V. By applying above sliding mode controller and based on the DC-DC converter topologies, it is possible to reach an expected voltage gain as shown in Figure 5.9. The DC bus voltage gain is seen to be stable at 2 pu for this case.

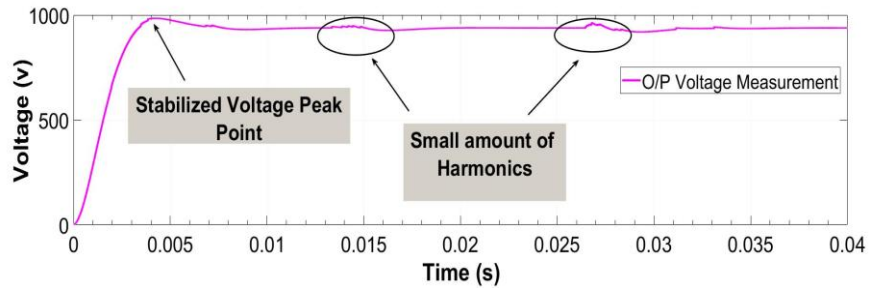


Figure 5.8. The output voltage of DC-DC converter.

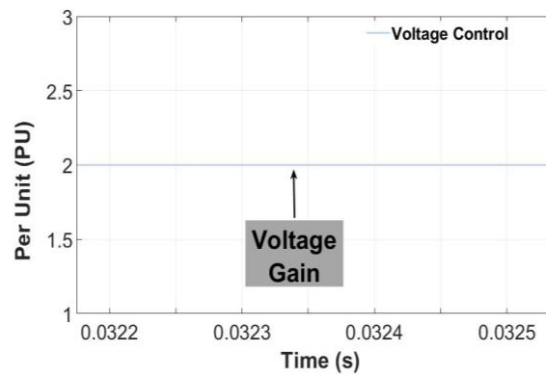


Figure 5.9. Voltage gain.

The steady state voltage of the fuel cell source achieved is less than 0.005 s (Figure 5.10). Output voltage is 938 V as noted here and reaches peak point by same time scale with small amount of harmonics that can be easily regulated. Additionally, it can be noted that the voltage becomes stabilized around 0.005 s at over 550 V. Figure 5.11 depicts the stabilized load voltage of a DC–DC converter. In this case, the voltage starts at 0 V and reaches a peak at 0.005 s. The peak voltage in this case is approximately 900 V.

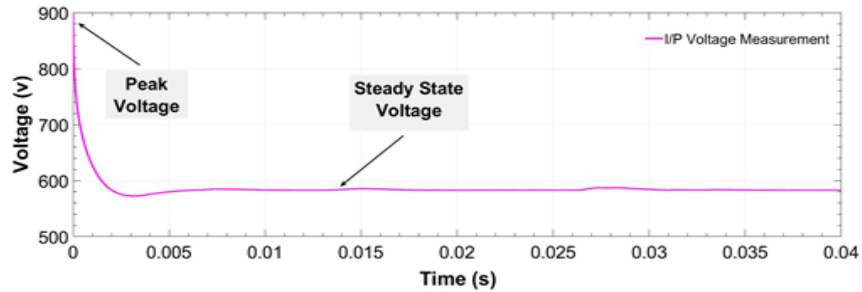


Figure 5.10. The source voltage of DC–DC converter.

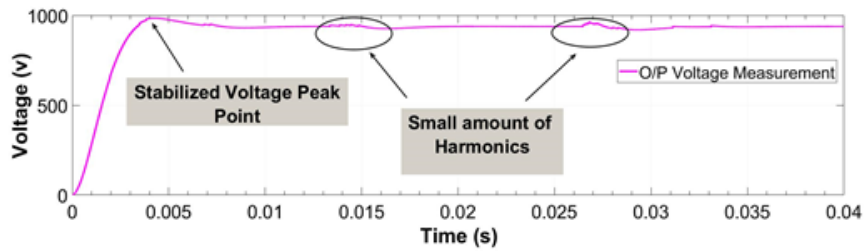


Figure 5.11. The stabilized load voltage.

Ripple current occurs because of the harmonics and measured input current= 250 A (Figure 5.12). Figure 5.12 has one ripple current which is indicated on the plot. Additionally, the current begins to stabilize around 0.01 s at 225 A. On the Figure 5.13, the output current is decreased by 100 A, although output ripple current is significantly reduced. Additionally, there is an output ripple current in this case as well. The current reaches a peak of 150 A at 0.005 s and then stabilizes to 140 A.

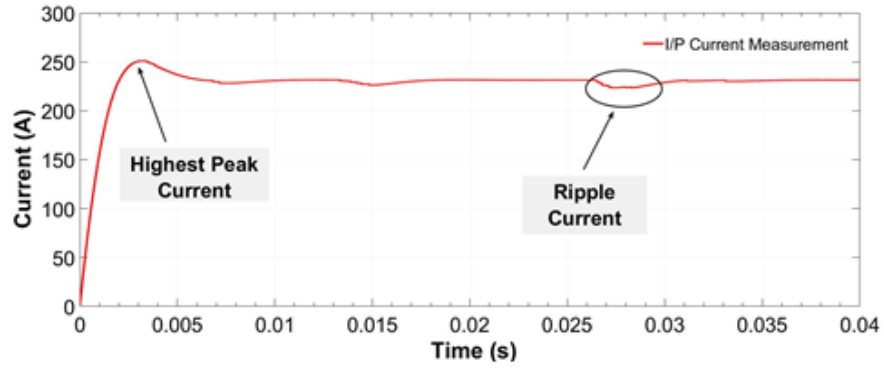


Figure. 5.12. Source current of DC–DC converter enclosed by lower current ripple.

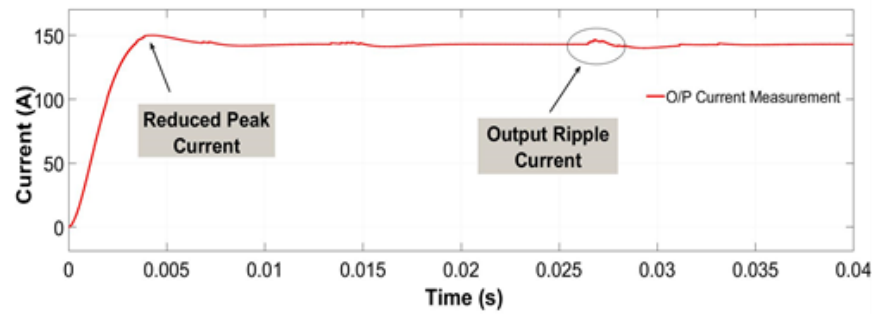


Figure 5.13. Load current of DC–DC converter.

Figure 5.14 shows converted output signal. Repeating output signal followed by data conversion rate robust and easy to regulate the output voltage can be easily gained.

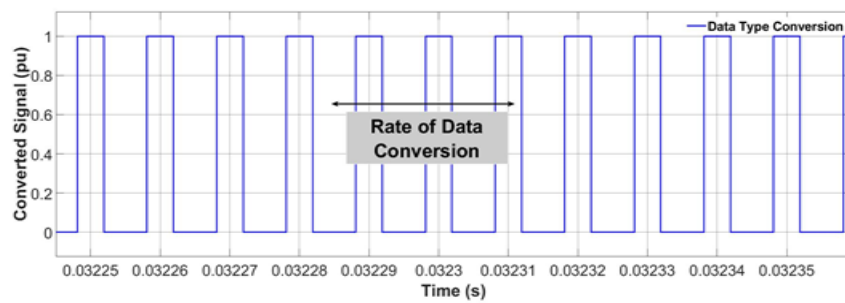


Figure 5.14. Converted signal of DC–DC converter.

Figure 5.15 shows a simulated PMSM DC–DC converter model for FCEV.

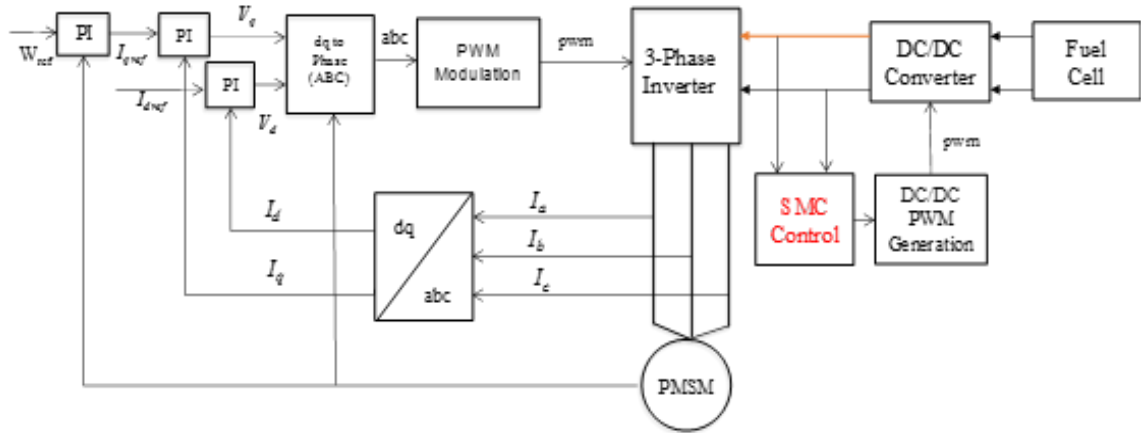


Figure 5.15. Simulated DC–DC converter control model for PMSM.

From Figures 5.16 and 5.17, it is seen that currents of the three phases are slightly unbalanced. Additionally, in Figure 5.16 the voltage of all three phases vary between -250 and $+250$ V. In Figure 5.17, the currents in all three phases vary between -10 and $+10$ A.

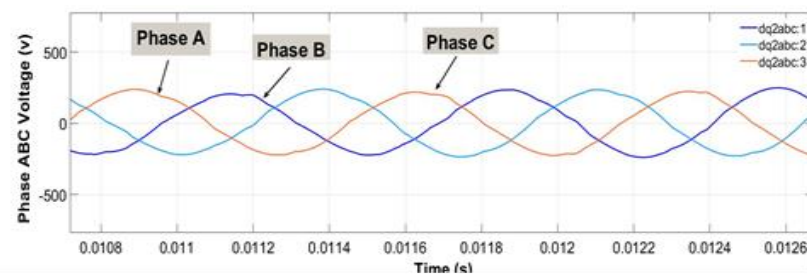


Figure 5.16. dq to phase voltage.

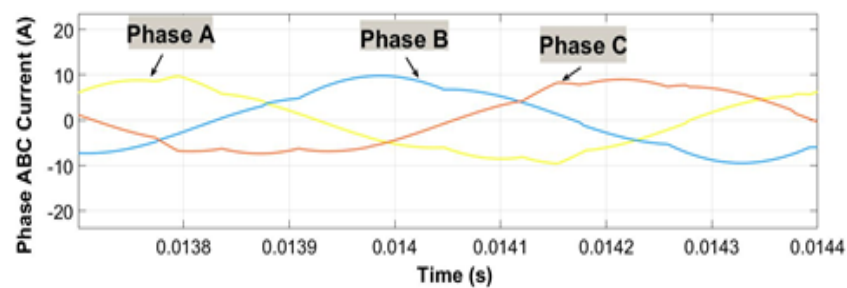


Figure 5.17. dq to phase current.

d -axis voltage is shown in Figure 5.18. From Figure 5.19, it is clearly observed that the d -axis current is higher compared to the q -axis current. From Figure 5.20, the peak torque is indicated on the plot and appears to be approximately 50 Nm.

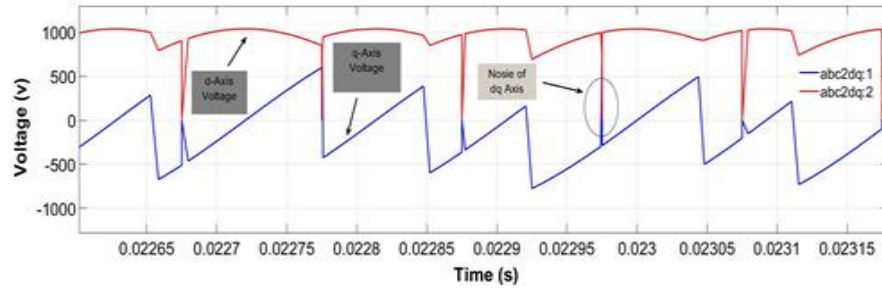


Figure 5.18. dq -axis voltage.

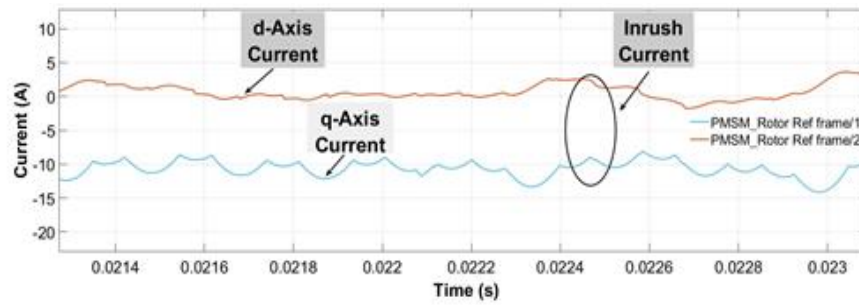


Figure 5.19. dq -axis current.

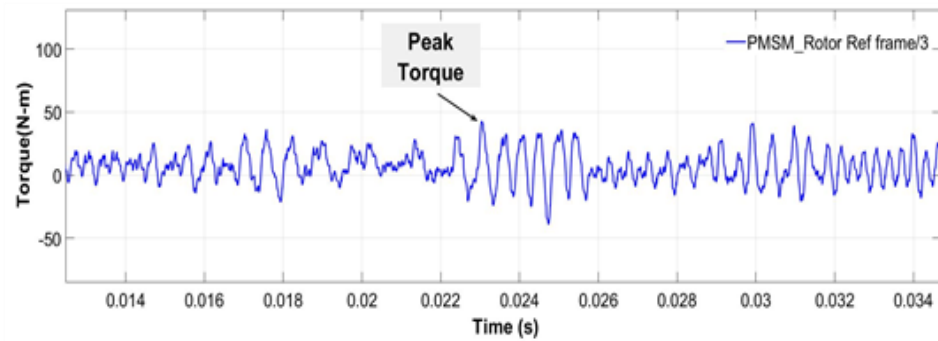


Figure 5.20. Electromagnetic torque.

Figure 5.21 shows the speed. The speed is analyzed for PMSM using PI controller. From this figure, the speed is seen to increase from 0 to 400 within 0.05 s.

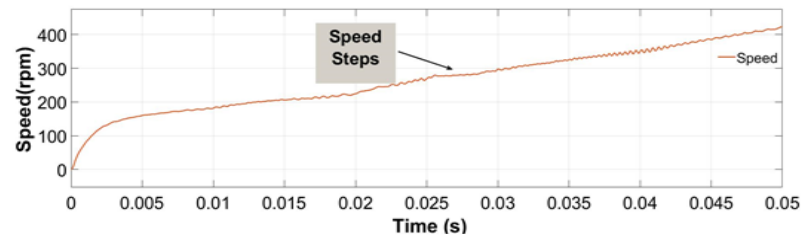


Figure 5.21. DC–DC converter control based on the rotor speed of PMSM.

CHAPTER 6

Conclusions and Future Work

6.1 Conclusions

Firstly, recent trend of fuel cell EV was introduced. Besides, the powertrain architecture of DC–DC converter behavior while in FCEV was briefly discussed. There are challenges with the system integration incorporating FC and power converter which were discussed thoroughly through circuitry analysis and showing that the continuous and discontinuous conduction effects of the DC–DC converter on the FC performance using existing literature.

Secondly, appropriate DC–DC converter topologies for FCEV application were discussed. Interleaved boost DC–DC converter, cascade boost DC–DC converter were studied. After investigation, limitations of the recently used DC–DC converter were identified. From that point of view, a suitable controller for the DC–DC converter was presented.

From the research presented in this thesis, it is shown that an FCEV can provide promising results when incorporated with a reliable and robust SMC. A DC–DC converter topology with the SMC control method is used in this thesis to demonstrate this. It is clear that the SMC can achieve accurate DC–bus voltage and power requirements.

DC–DC converter was studied under different operating conditions. The studied converter employs a two level boost converter and a two–level buck–boost converter in cascade to obtain a high voltage gain. It is shown that the converter operation ends up in low input current ripple. Simulation results demonstrate the applicability of the DC–DC converter, and show that high voltage gain is attainable, theoretically.

Finally, the controller of the DC–DC converter, which is comprised of multiple cascaded loops with low computational complexity, is utilized to boost and regulate the output DC voltage. The simulation results and the mathematical analysis using the existing literature shows that the proposed control scheme offers a robust coordination between the different functions of the DC–DC converter.

6.2 Future Work

This thesis studied different DC–DC converter topologies along with the controller's techniques used to interface the fuel cell to the motor controllers in FCEVs. The thesis discussed control strategies of DC–DC converter, yet the research area of powertrain control is rich with possibilities to find new ways to improve vehicle efficiency and increase the lifetime of the powertrain components through optimal control strategies of DC–DC converter. The future work can include a simple but practical boost DC–DC converter topology with a coordinated control that can improve converter performance under different operating conditions.

As a future work, it can be possible to build a robust universal DC–DC controller which could be applicable in FCEVs with any parameter varying condition. Furthermore, the study can be extended to include pure–electric vehicles, which can be powered by a battery or a battery and an ultracapacitor.

In terms of the higher–level vehicle optimization, investigations on the vehicle fuel economy, vehicle cost, control strategies specially for DC–DC converter, and the optimal sizing of components can be conducted.

REFERENCES/BIBLIOGRAPHY

- [1] C. C. Chen, A. Bouscayrol, and K. Chen, "Electric hybrid and fuel-cell vehicles: architectures and modeling," *IEEE Trans. on Veh. Tech.*, vol. 59, no. 2, pp. 589–598, 2010.
- [2] A. Khaligh and Z. Li, "Battery, ultracapacitor, fuel cell and hybrid energy storage systems for electric, hybrid electric, fuel cell and plug-in hybrid electric vehicles: State-of-the-art," *IEEE Trans. on Veh. Tech.*, vol. 59, no. 6, pp. 2806–2814, 2010.
- [3] H. K. Roy, A. McGordon, and P. A. Jennings, "A generalized powertrain design optimization methodology to reduce fuel economy variability in hybrid electric vehicles," *IEEE Trans. on Veh. Tech.*, vol. 63, no. 3, pp. 1055–1070, 2014.
- [4] V. F. Pires, A. Cordeiro, D. Foito, and J. F. Silva, "High step-up DC–DC converter for fuel-cell vehicles based on merged quadratic boost-cuk," *IEEE Trans. on Veh. Tech.*, vol. 68, no. 8, pp. 7521–7530, 2019.
- [5] C. M. Lai, Y. H. Cheng, M. H. Hsieh, and Y. C. Lin, "Development of a bidirectional DC–DC converter with dual-battery energy storage for hybrid electric vehicle system," *IEEE Trans. on Veh. Tech.*, vol. 67, no. 2, pp. 1036–1052, 2018.
- [6] Y. Zhang, L. Zhou, M. Summer, and P. Wang, "Single-switch wide voltage gain range, boost DC–DC converter for fuel cell vehicles," *IEEE Trans. on Veh. Tech.*, vol. 67, no. 1, pp. 134–145, 2018.
- [7] V. Ivanov, D. Savitski, and B. Shyrokau, "A survey of traction control and antilock braking systems of fuel cell electric vehicles with individually controlled electric motors," *IEEE Trans. on Veh. Tech.*, vol. 64, no. 9, pp. 3878–3896, 2015.
- [8] F. Zhang, X. Zhang, M. Zhang, and A. S. E. Edmonds, "Literature review of electric vehicle technology and its applications," in *proc. of IEEE Int. Conf. Comput. Sci. Netw. Tech.*, 2016.
- [9] T. Zhang, W. Chen, Z. Han, and Z. Cao, "Charging scheduling of electric vehicles with local renewable energy under uncertain electric vehicle arrival and grid power price," *IEEE Trans. on Veh. Tech.*, vol. 63, no. 6, pp. 2600–2612, 2014.
- [10] Z. Geng, T. Hong, K. Qi, J. Ambrosio, and D. Gu, "Modular regenerative emulation system for dc–dc converter in hybrid fuel cell vehicle applications," *IEEE Trans. on Veh. Tech.*, vol. 67, no. 10, pp. 9233–9240, 2018.
- [11] P. Wang, L. Zhou, Y. Zhang, J. Li, and M. Summer, "Input-parallel output-series dc–dc boost converter with a wide input voltage range, for fuel cell vehicle," *IEEE Trans. on Veh. Tech.*, vol. 66, no. 9, pp. 7771–7781, 2017.

- [12] M. Z. Hossain, N. A. Rahim, and J. Selvaraj, "Recent progress and developemets on power DC–DC convertre topology, control, design and applications: A review," in *proc. of IEEE Renewable and Sustainable Energy Reviews*, vol. 81, pp. 205–230, 2018.
- [13] N. Tanaka, "Technology Roadmap: Electric and plug–in hybrid electric vehicles," *IEEE Int. Energy Agency*, p. 52, 2011.
- [14] M. Klippenstein, "Fuel cell industry review," *Int. Canada EV sales:Green Tech Media*, 2017.
- [15] J. Chaben, "Canada fuel cell industry developments," In *FCHEA Fuel Cell & Hydrogen Energy Association*, Aprl. 2019.
- [16] S. Basu, *Recent Trends in Fuel Cell Science and Technology*, Springer, Book, no. 375, 2007.
- [17] Global Market Watch, "Global fuel cell market 2020," Dec. 2019.
- [18] B. M. Reddy and P. Samuel, "Technology advancements and trendsin development of proton exchange membrane fuel cell hybrid electric vehicles," *IEEE Trans. on Green Energy.*, vol. 7, no. 3, 2017.
- [19] D. Ravi, S. S. Letha, P. Samual, and B. M. Reddy, "An overview of various DC–DC converter techniques used for fuel cell based applications," in *proc. of. IEEE Int. Conference. on Power Energy, Environment and Intelligent Control (PEEIC)*, 2019.
- [20] O. Hegazy, J. V. Mierlo, and P. Lataire, "Analysis, control and implementation of a high–power interleaved boost converter for fuel cell hybrid, electric vehicle," *IEEE Int. Rev., Electr., Eng.*, vol. 6, no. 4, pp. 1739–1747, 2011.
- [21] J. Marshall and M. Kazerani, "Design of an efficient fuel cell vehicle drivetrain, featuring a novel boost converter," in *proc. of IEEE 31st Annual Conference of Industrial Electronics Society (IECON)*, pp. 1–6, 2005.
- [22] A. Payman, S. Pierfederici, and F. Meibody–Tabar, "Energy management in a fuel cell/supercapacitor multisource/multiload electrical hybrid system," *IEEE Trans. on Power Electron.*, vol. 24, no. 12, pp. 2681–2690, 2009.
- [23] Z. Bostao, W. Qi, Z. Min, and H. Huan, "Analysis solution for the inductor current of boost converter," *IEEE Power Electronics (IET)*, vol. 12, pp. 2424–2432, 2019.
- [24] P. Sleski, E. Janicka, K. Darowicki, and B. Pierozynski, "Impedance monitoring of fuel cell stack," *IEEE Journal of Solid State Electrochemistry*, vol. 19, pp. 929–933, 2015.
- [25] S. M. Nijoya and L. T. Olivier, "A generic fuel cell model for the simulation of fuel cell vehicles," in *proc. of IEEE Conference of Vehicle Power and Propulsion (VPPC)*, pp. 1–

6, 2009.

- [26] Z. L. Jiang *et al.*, “Energy management for a fuel cell hybrid vehicle,” in *proc. of IEEE Conference of Asia–Pacific Power and Energy Engineering (APPEEC)*, pp. 1–6, 2010.
- [27] M. Venturi, C. Mohrdieck, and J. Friedrich, “Mercedes–Benz b–class fuel cell: the world largest hydrogen vehicle fuel cell fleet experience,” in *proc. of IEEE Conference of Electric Vehicle Symposium and Exhibition (EVS)*, pp. 1–6, 2013.
- [28] A. B. Ki and T. W. Lim, “Fuel cell vehicle development at Hyundai–Kia Motors,” in *proc. of IEEE 1st International Forum on Strategic Technology*, pp.1–6, 2006.
- [29] S. Mekhilef, R. Saidur, and A. Safari, “A Comparative study of different fuel cell technologies,” *IEEE Renew Sustain Energy Rev.*, vol. 16, no. 1, pp. 981–987, 2012.
- [30] A. Stambouli and Boudghene, “Traversa E. Fuel cells, an alternative to standard sources of energy,” *IEEE Renew Sustain Energy Rev.*, vol. 6, no. 1, pp. 295–304, 2002.
- [31] Arif Ahmed *et al.*, “Ammonia–fed fuel cells: a comprehensive review,” *IEEE Renew Sustain Energy Rev*, vol. 60, no. 1, pp. 822–835, 2016.
- [32] M. Thomas *et al.*, “Feasibility study of 2020 target costs for PEM fuel cells and lithium–ion batteries: a two–factor experience curve approach,” *IEEE International. J. Hydro Energy*, vol. 37, no. 19, pp. 14463–14474, 2012.
- [33] Z. S. Omar and M. F. Orhan, “An overview of fuel cell technology: fundamentals and applications,” *IEEE Renew Sustain Energy Rev.*, vol. 32, no. 3, pp. 810–853, 2014.
- [34] S. Jose and L. A. Gomes, “Fuel cell cogeneration system: A case of techno economic analysis,” *IEEE Renew Sustain Energy Rev.*, vol. 3, no. 2, pp. 233–242, 1999.
- [35] A. Choudhury, H. Chandra, and A. Arora, “Application of solid oxide fuel cell technology for power generation,” *IEEE Renew Sustain Energy Rev.*, vol. 20, no. 1, pp. 430–442, 2013.
- [36] A. Kirubakaran, J. Shailendra, and R. K. Nema, “A review on fuel cell technologies and power electronics interface,” *IEEE Renew Sustain Energy Rev.*, vol. 13, pp. 2430–440, 2009.
- [37] N. Sulaiman *et al.*, “A review on energy management system for fuel cell hybrid electric vehicles: issues and challenges,” *IEEE Renew Sustain Energy Rev.*, vol. 52, no. 1, 2015.
- [38] H. Mustapha, A. Meharrar, and M. Tioursi, “Power management strategy in the alternative energy /PEM fuel cell hybrid system,” *IEEE Renew Sustain Energy Rev.*, vol. 15, no. 9, pp. 5104–5110, 2011.
- [39] C. Wang, M. H. Nehrir, and S. R. Shaw, “Dynamic models and model validation for PEM fuel cells using electrical circuits,” *IEEE Transactions on Energy Conversion*, vol. 20, no.

- 2, pp. 442–451, 2005.
- [40] A. Forrai and Y. Yanagit, “Fuel cell parameter estimation and diagnostics,” *IEEE Transactions on Energy Conversion*, vol. 20, no. 3, pp. 668–675, 2005.
 - [41] A. Hajizadeh and A. G. Masoud, “Intelligent power management strategy of hybrid distributed system,” *IEEE International Journal of Electrical Power & Energy Systems*, vol. 29, 2007.
 - [42] F. M. Ronald *et al.*, “Development and application of a generalized steady-state electrochemical model for a PEM fuel cell,” *IEEE J. Power Sources*, vol. 86, no. 1, pp. 173–80, 2000.
 - [43] C. Alben, A. Kodjo, and H. Nislson, “Development of power interface with FPGA-based adaptive control for PEM-FC system,” *IEEE Trans. Energy Convers.*, vol. 30, no. 1, pp. 296–306, 2015.
 - [44] L. C. Iwan and F. S. Robert, “The application of neural networks to fuel processors for fuel-cell vehicles,” *IEEE Trans. Veh. Tech.*, vol. 50, no. 1, pp. 125–43, 2001.
 - [45] S. H. Abdi *et al.*, “A novel approach for robust maximum power point tracking of PEM fuel cell generator using sliding mode control approach,” *IEEE International. J Electrochemical Sci.*, vol. 7, no. 1, pp. 4192–209, 2012.
 - [46] H. X. Song *et al.*, “Optimal dimensioning and power management of a fuel cell/battery hybrid bus via convex programming,” *IEEE Trans. Mechatronics*, vol. 20, no. 1, pp. 457–468, 2015.
 - [47] W. Yun *et al.*, “A review of polymer electrolyte membrane fuel cells: technology, applications, and needs on fundamental research,” *IEEE Appl. Energy*, vol. 88, no. 4, pp. 981–1007, 2011.
 - [48] N. Mohan, T. M. Undulant, and W.P. Robbins, *Power Electronics: Converters, Applications, and Design*, John Wiley & Sons, 3rd edition, 2001.
 - [49] J. H. Hirschhofer, “Fuel cell status,” *IEEE Trans. of Aerospace Electron Syst. Mag.*, vol. 9, no. 11, pp. 10–5, 1994.
 - [50] R. W. Erickson and D. Maksimovic, *Fundamental of Power Electronics*, Kluwer Academic, Boston, Mass, USA, 2nd edition, 2001.
 - [51] O. Hegazy, J. V. Mierlo, and P. Lataire, “Analysis modeling and implementation of a multiservice interleaved DC–DC converter for fuel cell hybrid electric vehicles,” *IEEE Trans. of Power Electron.*, vol. 27, no. 11, pp. 4445–4458, 2012.
 - [52] M. Muhammad, M. Armstrong, and M. A. Elgendy, “A non-isolated interleaved boost

- converter for high-voltage gain applications,” *IEEE J. Emerge. Sel. Top. Power Electron.*, vol. 4, no. 2, pp. 352–362, 2016.
- [53] Y. T. Chen, Z. M. Li, and R. H. Liang, “A novel soft-switching interleaved coupled-inductor boost converter with only single auxiliary circuit,” *IEEE Trans., of Power Electron.*, vol. 33, no. 3, pp. 2267–2281, 2018.
 - [54] W. Khadmun, and W. Subingha, “High voltage gain interleaved DC boost converter application for photovoltaic generation system,” *IEEE Eco-Energy and Material Science and Engineering (EMSES)*, vol. 34, pp. 390–398, 2013.
 - [55] T. Nouri, N. Vosoghi, and S. H. Hossein, “An interleaved high step-up with coupled inductor and built-in transformer voltage multiplier cell techniques,” *IEEE Trans. on Industrial Elec.*, vol. 66, no. 3, pp. 1894–1905, 2018.
 - [56] D. Makimovic, J. Chen, and R. Erickson, “Buck-boost PWM converters having two independently controlled switches,” in *proc. of IEEE 32nd Annual Conference of Power Elec., Specialists*, pp. 736–741, 2001.
 - [57] Hwang *et al.*, “A low-voltage positive buck-boost converter using average-current-controlled techniques,” in *proc. of IEEE International Symposium on Circuits and Systems (ISCAS)*, pp. 2255–2258, Seoul, Republic of Korea, 2012.
 - [58] K. I. Hwu and Y. T. Yau, “A novel voltage-boosting converter,” pp. 368–372, 2007.
 - [59] Y. T. Yau and K. I. Hwu, “Inductor-coupled KY boost converter,” *IEEE Electron. Lett.*, vol. 46, no. 24, pp. 24–25, 2010.
 - [60] K. I. Hwu *et al.*, “Inductor-coupled KY boost converter,” *Electron. Lett.*, vol. 46, no. 24, pp. 24–25, 2010.
 - [61] X. Feng, J. Liu, and F.C. Lee, “Impedance specifications for stable DC distributed power system,” *IEEE Trans. Power Electron.*, vol. 17, no. 2, pp. 157–162, 2002.
 - [62] S. Y. Tseng, S. H. Tseng, and J. Z. Shiang, “High step-up converter associated with soft-switching circuit with partial energy processing for livestock stunning applications,” in *proc. of IEEE 5th Int. Conference of Power Electron. Motion Control*, pp. 1086–1090, 2007.
 - [63] B. R. Lin and C. L. Huang, “Analysis and implementation of a soft switching converter with high-voltage conversion ratio,” *Int. Rev. Elec. Eng.*, vol. 6, no. 7, pp. 2846–2852, 2011.
 - [64] M. Lotif *et al.*, “New cascade boost converter with reduced losses,” *IEEE IET Power Electron.*, vol. 9, no. 6, pp. 1213–1219, 2016.

- [65] S. W. Lee and H. L. Do, "High step-up coupled inductor cascade boost DC-DC converter with lossless passive snubber," *IEEE Trans. Ind. Elec.*, vol. 65, no.10, pp. 7753–7761, 2018.
- [66] O. Ellabban *et al.*, "Dual loop digital control design and implementation of a DSP based high power boost converter in fuel cell electric vehicle," in *proc. of IEEE Conference of OPTIM*, 2010.
- [67] S. Buso and P. Mattavelli, *Digital Control in Power Electronics*, Morgan and Claypool Publishers, 2006.
- [68] H. Xu, E. Qiao, X. Guo, X. Wen, and L. Kong, "Analysis and design of high power interleaved boost converters for fuel cell distributed generation system," in *proc. of IEEE Conference of Power Electron. Spec.*, pp 140–145, 2005.
- [69] B. Huang, A. Shahin, J. P. Matin, S. Pierfederici, and B. Davat, "High voltage ratio non-isolated DC-DC converter for fuel cell power source applications," in *proc. of IEEE Conference of Power Electron. Spec.*, pp. 1277–1283, 2008.
- [70] P. Liutanakul *et al.*, "Stability investigation of inverter motor drive system with input filter-Optimization of the DC-link capacitance value," in *proc. of IEEE Conference of Power Electron. Spec.*, pp. 3728–3734, 2008.
- [71] M. F. M. Sabri, K. A. Danapalasingam, and M. F. Rahmat, "A review on hybrid electric vehicles architecture and energy management strategies," *Renewable and Sustainable Energy Reviews*, vol 53, pp. 1433–1442, 2016.
- [72] B. R. Lin and J. Y. Dong, "New zero-voltage switching DC-DC converter for renewable energy conversion system," *IET Power Electronics*, vol. 5, no.4, pp.393–400, 2012.
- [73] T. Phatiphat *et al.*, "Intelligent model-based control of a standalone fuel cell power plant with supercapacitor energy storage," *IEEE Trans. Sustain Energy*, vol. 4, no. 1, 2013.
- [74] W. Khadmun and W. Subsingha, "High voltage gain interleaved DC boost converter application for photovoltaic generation system," *Energy Procedia*, vol. 34, pp. 390–398, 2013.
- [75] M. Derbeli, L. Sbita, M. Farhat, and O. Barambones, "Proton exchange membrane fuel cells – A smart drive algorithm," in *proc. of IEEE Conference in Green Energy Conversion Systems (GECS)*, vol. 17, no. 1, pp.1–5, 2017.
- [76] C. Aliotta, L. Liotta, F. Deganello, V. La Parola, and A. Martorana, "Direct methane oxidation as potential anode for intermediate temperature solid oxide fuel cells," *Applied Catalysis B: Environmental*, vol. 180, pp. 424–433, 2016.

- [77] F. D. Bianchi, C. Ocampo–Martinez, C. Kunusch, and R. S. Sanchez–Pena, “Fault–tolerant unfalsified control for PEM fuel cell system,” *IEEE Trans. on Energy Conversion*, vol. 30, no. 1, pp. 307–315, 2015.
- [78] E. Hosseinzadeh, M. Rokni, S. G. Advani, and A. K. Prasad, “Performance simulation and analysis of a fuel cell/battery hybrid forklift truck,” *IEEE International Journal of Hydrogen Energy*, vol. 38, no.11, pp. 4241–4249, 2017.
- [79] M. Uzunoglu and M. S. Alam, “Dynamic modeling, design and simulation of a PEM fuel cell/ultra–capacitor hybrid system for vehicular applications,” *IEEE Energy Conversion and Management*, vol. 48, no. 5, pp. 1544–1553, 2007.
- [80] Y. He and F. Luo, “Study of sliding mode control for DC–DC converters,” in *proc. of IEEE International Conference on Power System Technology*, vol. 2, pp. 1969–1974, 2004.
- [81] M. Derbeli, L. Sbita, M. Farhat, and O. Barambones, “PEM fuel cell green energy generations efficiency optimization,” in *proc. of IEEE International Conference on Green Energy Conversion Systems (GECS)*, pp. 1–5, 2017.
- [82] O. Lopez–Lapena, M. T. Penella, and M. Gasulla, “A new MPPT method for low–power solar energy harvesting,” *IEEE Transactions on Industrial Electronics*, vol. 57, no. 9, pp. 3129–3138, 2010.
- [83] A. Cid–Pastor *et. al.*, “Synthesis of loss–free resistors based on sliding–mode control and its applications in power processing,” *IEEE Control Engineering Practice*, vol. 21, no. 5, pp. 689–699, 2013.
- [84] S. Dwari and L. Parsa, “A novel high efficiency high power interleaved coupled–inductor boost DC–DC converter for hybrid and fuel cell electric vehicle,” in *proc. of IEEE Vehicle Power and Propulsion Conference (VPPC)*, pp.399–404, 2007
- [85] H. Xu *et al.*, "High power interleaved boost converter in fuel cell hybrid electric vehicle," in *proc. of IEEE International Conference on Electric Machines and Drives*, vol. 128, no.11, pp.1814–1819,2005.
- [86] A. H. M Yatim *et al.*, “Dynamic evolution controller for single phase inverter application,” in *proc. of IEEE Symposium on Industrial Electronics & Applications (ISIEA)*, pp.530–535, 2009.
- [87] J. Wen and T. Smedley, "A new interleaved isolated boost converter for high power applications," in *proc. of IEEE Applied Power Electronics Conference and Exposition (APEC)*, 2006.
- [88] C. Chunliu *et al.*, “Research of an interleaved boost converter with four interleaved boost

- convert cells," in *proc. of IEEE Asia Pacific Conference on Postgraduate Research*, pp. 396–399, 2009.
- [89] A. S. Samosir and A. H. M. Yatim, "Implementation of new control method based on dynamic evolution control with linear evolution path for boost DC–DC converter," *Power and Energy Conference*, in *proc. of IEEE International Conference of European Union (ICE)*, 2008.
 - [90] Z. Zhang, *et al.*, "Interleaved half bridge dual-input DC-DC converter with a PWM plus phase-shift control for fuel cell applications" *IEEE 39th Annual Conference of the Industrial Electronic Society (IECON)*, 2013.
 - [91] Y. X. Wang *et al.*, "Robust time–delay control for the DC–DC boost converter," *IEEE Trans. Industrial Electronics*, vol. 61, no. 9, pp. 4829–4837, 2014.
 - [92] Y. Huangfu *et al.*, "Robust voltage control of floating interleaved boost converter for fuel cell systems," *IEEE Transactions on Industry Applications*, vol. 54, no. 1, pp. 665–674, 2018.
 - [93] Q. Li *et al.*, "Controller design and fault tolerance analysis of 4–phase floating interleaved boost converter for fuel cell electric vehicles," in *proc. of IEEE 3rd Annual Conference of IECON*, 2017.
 - [94] Y. Son *et al.*, "Complementary PID controller to passivity–based nonlinear control of boost converters with inductor resistance," *IEEE Trans. on Control Systems Tech.*, vol. 20, pp. 826–834, 2012.
 - [95] P. Thounthong, P. Tricoli, and B. Davat, "Performance investigation of linear and nonlinear controls for a fuel cell/super–capacitor hybrid power plant," *IEEE International Journal of Electrical Power & Energy Systems*, vol. 54, pp. 454–464, 2014.
 - [96] B. Wang *et al.*, "Duty–ratio based adaptive sliding–mode control method for boost converter in a hybrid energy storage system," *IEEE Energy Procedia*, vol. 105, pp. 2360–2365, 2017.
 - [97] M. Zandi *et al.*, "Flatness based control of a non–ideal DC–DC boost converter," in *proc. of IEEE Annual Conference on Industrial Electronics Society (IECON)* 2011.
 - [98] P. Thounthong *et al.*, "Modeling and control of fuel cell/super capacitor hybrid source based on differential flatness control," *IEEE Transactions on Vehicular Technology*, vol. 59, no. 6, pp. 2700–2710, 2010.
 - [99] I. M. Safwat *et al.*, "Adaptive fuzzy logic control of boost converter fed by stand–alone PEM fuel cell stack," in *proc. of IEEE Transportation Electrification Asia–Pacific (ITEC*

Asia-Pacific), 2017.

- [100] P. Thounthong, *et al.*, “Control of a three-level boost converter based on a differential flatness approach for fuel cell vehicle applications,” *IEEE Transactions on Veh. Technology*, vol. 61, no. 3, pp. 1467–1472, 2012.
- [101] B. Salhi *et al.*, “Adaptive output feedback control of interleaved parallel boost converters associated with fuel cell,” *Electric Power Components and Systems*, vol. 43, pp. 1141–1158, 2015.
- [102] S. Oucheriah and L. Guo, “PWM-based adaptive sliding-mode control for boost DC–DC converters,” *IEEE Transactions on Industrial Electronics*, vol. 60, no. 8, pp. 3291–3294, 2013.
- [103] B. Wang *et al.*, “Implementation of an estimator-based adaptive sliding mode control strategy for a boost converter based battery/super capacitor hybrid energy storage system in electric vehicles,” *IEEE Energy Conversion and Management*, vol. 151, pp. 562–572, 2017.
- [104] A. Shahin *et al.*, “Approximate novel loss formulae estimation for optimization of power controller of DC–DC converter,” *IEEE Annual Conference on Industrial Electronics Society (IECON)*, 2010.
- [105] S. Hamedani *et al.*, “Flatness-based control method: A review of its applications to power systems,” in *proc. of IEEE Power Electronics and Drive Systems Technologies Conference (PEDSTC)*, 2016.
- [106] A. Payman *et al.*, “Energy control of super capacitor/fuel cell hybrid power source,” *IEEE Energy Conversion and Management*, vol. 49, pp. 1637–1644, 2008.
- [107] H. Armghan, I. Ahmad, A. Armghan, S. Khan, and M. Arsalan, “Back–stepping based non–linear control for maximum power point tracking in photovoltaic system,” *IEEE Sol. Energy*, vol. 159, pp. 134–141. 2018.
- [108] H. Armghan, I. Ahmad, N. Ali, M. F. Munir, S. Khan, and A. Armghan, “Nonlinear controller analysis of fuel cell battery ultracapacitor–based hybrid energy storage systems in electric vehicles,” *IEEE Arabian J. Sci. Eng.*, vol. 43, no. 6, pp. 3123–3133, 2018.
- [109] J. Cao and A. Emadi, “A new battery/ultracapacitor hybrid energy storage system for electric, hybrid, and plug–in hybrid electric vehicles,” *IEEE Trans. Power Elec.*, vol. 27, no. 1, pp. 122–132, 2012.
- [110] F. Akar, Y. Tavlasoglu, E. Ugur, B. Vural, and I. Aksoy, “A bidirectional non isolated multi–input DC–DC converter for hybrid energy storage system in terms of electric

- vehicles,” *IEEE Trans. Veh. Tech.*, vol. 65, pp. 7944–7955, 2015.
- [111] L. Solero, A. Lidozzi, and J. A. Pomilio, “Design of multiple–input power converter for hybrid vehicles,” *IEEE Trans. Power Elec.*, vol. 20, no. 5, pp. 1007–1016, Sep. 2005.
 - [112] R. Ferreira, A. Ferreira, and P. Barbosa, “Comparative study of linear and non–linear control techniques applied to DC–DC boost converter as a voltage regulator,” *IEEE Tech. Rep.*, vol. 7, pp. 331–385, 2018.
 - [113] O. L. Santos *et al.*, “Robust sliding mode control design for a voltage regulated quadratic boost converter,” *IEEE Trans. Power Electron*, vol. 30, no. 4, pp. 2313–2327, 2015.
 - [114] M. S. Khan, I. Ahmad, H. Armaghan, and N. Ali, “Backstepping sliding mode control of FC–UC based hybrid electric vehicle,” *IEEE Access*, vol. 6, pp. 77202–77211, 2018.
 - [115] H. El–Fadil, F. Giri, J. M. Guerrero, and A. Tahri, “Modeling and nonlinear control of a fuel cell/supercapacitor hybrid energy storage system for electric vehicle,” *IEEE Trans. Veh. Tech.*, vol. 63, no. 7, pp. 3011–3018, Sep. 2014.
 - [116] M. Mohammedi, O. Kraa, M. Becherif, A. Aboubou, M. Ayad, and M. Bahri, “Fuzzy logic and passivity–based controller applied to electric vehicle using fuel cell and supercapacitors hybrid source,” *IEEE Tran. Of Energy Conversion.*, vol. 50, pp. 619–626, Jan. 2014.
 - [117] L. K. Yi, J. Zhao, and D. Ma, “Adaptive backstepping sliding mode nonlinear control for buck DC–DC switched power converter,” in *proc. of IEEE Int. Conf. Control Autom.*, pp. 1198–1201, 2007.
 - [118] R. Skjetne and T. I. Fossen, “An integral control in backstepping: Analysis of different techniques,” in *proc. of IEEE Control Conf.*, vol. 2, pp. 1899–1904, 2004.
 - [119] J. Liu, Y. Gao, X. Su, M. Wack, and L. Wu, “Disturbance–observer– based control for air management of PEM fuel cell systems via sliding mode technique,” *IEEE Trans. Control Syst. Tech.*, vol. 27, no. 3, pp. 1129–1138, 2019.
 - [120] O. P. Jaga and S. K. Maurya, “Modeling and control strategies for energy management system in electric vehicles,” *IEEE Perspect. Sci.*, vol. 8, pp. 358–360, 2016.
 - [121] H. Sharma, O. P. Jaga, and S. K. Maurya, “Dynamic evolution control strategies for FC System,” 2016.
 - [122] O. Lopez–Santos, L. Martinez–Salamero, G. Garcia, H. Valderrama–Blavi, and T. Sierra–Polanco, “Robust sliding–mode control design for a voltage regulated quadratic boost converter,” *IEEE Trans. Power Elec.*, vol. 30, no. 4, pp. 2313–2327, 2015.
 - [123] P. D. Reddy and B. Banakar, “Sliding mode control technique for DC–DC buck–boost

- converter,” *IEEE Trans. of Power Elec.*, vol. 3, no. 12, pp. 271–280, 2015.
- [124] H. Sira–Ramirez and R. Silva–Ortigoza, *Control Design Techniques in Power Electronic Devices*, Springer 1st Ed., Berlin, Germany, 2006.
 - [125] H. F. Giri, *et. al.*, “Adaptive sliding mode control of interleaved parallel boost converter for fuel cell energy generation system,” *IEEE Trans. on Mathematics and Computer Simulation (ELESVIER)*, vol. 9, pp. 193–210, 2013.
 - [126] H. Sharma, O. P. Jaga, and S. K. Maurya, “Sliding mode control strategies for FC system,” *IEEE Trans. on Power Elec.*, vol. 24, pp. 14–18, 2010.
 - [127] O. P. Jaga and S. K. Maurya, “Modeling and control strategies for energy management system in electric vehicles,” *IEEE Prospect Sci.*, vol. 8, pp. 358–360, 2010.
 - [128] H. Sharma, O. P. Jaga, and S. K. Maurya, “Dynamic evolution control strategies for FC system,” *IEEE Trans. on Power Elec.*, vol. 13, pp. 251–271, 2016.
 - [129] F. Z. Belhaj *et. al.*, “Sliding mode control of a cascade boost converter for fuel cell energy generation system,” *IEEE Conference on Electrical and Information Technologies (ICEIT)*, 2017.
 - [130] Z. Chen, “PI and sliding mode control of a Cuk converter,” *IEEE Trans. Power Electron.*, vol. 27, no. 8, pp. 3695–3703, 2012.
 - [131] A. Y. Kamik, J. H. Buckland, and J. Sun, “Performance of a PEM fuel cell water management system using static output feedback,” *IEEE Trans. of Power Elec.*, pp. 2997–3002, 2007.
 - [132] A. Tiwari and O. P. Jaga, “Component selection for an electric vehicle: A comparative study,” *IEEE International Conference on Computation of Power, Energy Information and Communication (ICCPEIC)*, 2017.
 - [133] E. L. Fahdi and J. M. Guerrero, “Sliding mode control of fuel cell and supercapacitor hybrid energy storage system,” in *proc. of IEEE Conference of IFAC Symposium on Power Plants and Power System Control (PPPSC)*, 2012
 - [134] H. E. Fadil *et. al.*, “Modeling and nonlinear control of a fuel cell /supercapacitor hybrid storage system for electric vehicles,” *IEEE Trans., on Veh., Tech.*, vol. 63, no. 7, pp. 3011–3018, 2014.
 - [135] J. M. Guerrero *et. al.*, “Adaptive sliding mode control of interleaved parallel boost converter for fuel cell energy sources,” in *proc. of IEEE ELECTRIMACS Conference*, 2011.
 - [136] E. L. Maguiri *et. al.*, “Adaptive output regulation of series resonant DC–DC converters: A combined sliding mode and backstepping control design,” in *proc. of IEEE European*

Control Conference (ECC), 2009.

- [137] E. L. Fadil and F. Giri, “Reducing chattering phenomenon in sliding mode control of buck–boost power converters,” in *proc. of IEEE International Symposium in Industrial Electronics (ISIE)*, 2008.

VITA AUCTORIS

NAME: Pronay Kumar Chakrobarty

PLACE OF BIRTH: Rajbari, Dhaka, Bangladesh

YEAR OF BIRTH: 1989

EDUCATION: 2020: Master of Applied Science in Electrical and
Computer Engineering (MASc), University of
Windsor, Windsor, ON, Canada

2015: Bachelor of Science in Electrical and
Electronic Engineering (BSc), American
International University–Bangladesh (AIUB),
Dhaka, Bangladesh

2008: Higher Secondary School Certificate (HSC) in
Science Group, Rajbari Govt. College, Rajbari,
Dhaka, Bangladesh